MODELING OF COMPOSITE SHELLS IN 6–PARAMETER NONLINEAR THEORY WITH DRILLING DEGREE OF FREEDOM

ABSTRACT

Within the framework of a 6-parameter nonlinear shell theory, with strain measures of Cosserat type, constitutive relations are proposed for thin elastic composite shells. The material law is expressed in terms of five engineering constants of classical anisotropic continuum plus an additional parameter accounting for drilling stiffness. The theory allows for unlimited displacements and rotations. A number of examples are presented to show the correctness of the proposed model.

KEYWORDS: 6–PARAMETER SHELL THEORY, COMPOSITE SHELLS, SHELL INTERSECTIONS

1. INTRODUCTION

The aim of this paper is to propose constitutive relations for composite shells within the framework of 6-parameter shell theory with drilling degree of freedom. One of the disputable issues of this theory, and the finite elements that introduce the sixth degree of freedom, is the question of constitutive relation for the drilling resultants or selection of appropriate stiffness in FEM approach.

In this paper we propose the simplest (primitive) approach that would throw some light on the nature of the drilling degree of freedom in composite shells. Our approach (based on previous experiences with homogenous isotropic shells [1], [2], [3], [4]) is a straightforward extension of well-known concepts from 5-parameter theory.

We assume that the constitutive equation for the drilling resultant is obtained as a result of integration over the shell thickness. In the limit case, assuming single layer shell, the derived equation should yield the equations written in previous works (see [1], [2], [3], [4] and references given therein). In addition, the numerical results obtained with the proposed formulation should be confirmed by classical results from 5-parameter theory, wherever the agreement should hold.

The most important characteristics of the shell theory employed here are:

- The theory is statically exact, i.e. the exact 2D equilibrium equations of the shell-like body are derived by direct through-the-thickness integration of 3D balance laws of linear and angular momentum of the Cauchy continuum.
- The two vector equilibrium equations are expressed in terms of resultant quantities, so from the computational viewpoint there is no necessity of integration over the element volume, which is typically required for the degenerated elements.
- The theory is kinematically exact meaning that the shell kinematics is a direct implication of an integral identity resulting from the exact equilibrium equations derived as specified above. The resulting kinematic model is

formally equivalent to the Cosserat surface with three rigidly rotating directors. The drilling degree of freedom appears as a direct consequence of the applied theoretical shell model.

- The kinematics of the shell is described by the field of generalized displacements, composed of the translation vector field and the rotation tensor field both being independent variables. The presence of rotation tensor causes that the sixth degree of freedom appears consequentially at each node of the FEM mesh.
- The theory allows for unlimited translations and rotations and it accommodates naturally various geometric irregularities such as, for example, folds, branches and/or intersections.

A detailed introduction to the theory can be found for instance in the works of Reissner [5], Libai and Simmonds [6] and Chróścielewski et al. [1]. The formulations of appropriate shell finite elements and associated computational aspects have been discussed, among others, in [2], [3], [4]. In particular, in [2] the finite translation/rotation elements named CAM with 4-, 9- and 16-node were elaborated. In this paper we purposely use the bi-cubic (16-node) CAM elements based on the 'pure' generalized displacement (translation/rotation) formulation. Therefore, additional issues concerned with the theory and approximation are not introduced as in a case for example of hybrid elements, assumed natural strain elements, mixed elements and corresponding finite element approximation, cf. for instance [4], [7], [8][7][8]. Since the sixth parameter in the present theory is the drilling rotation the important effect of Poisson thickness locking, see for instance [9] or [10] and references given therein, does not occurs here.

Interested readers can find numerous papers dealing successfully with both constructing the theory of shells with drilling dof and its implementation, choosing the rotation parameterization and allowing for general elastic or inelastic constitutive equations, see for instance[11], [12], [13],[14],[15],[16],[17],[18],[19],[20],[21].

The authors of the present paper made an attempt to exploit their earlier experience in constructing 6 dof models for isotropic shells [3][4] and 5 dof models for composite shells [22][23] to create a new computational model with independent three translations and three rotational parameters capable of dealing with composite shells possessing irregular (non-smooth) reference surfaces. The computational model of material of the composite shell is constructed in the present paper by adopting the following assumptions:

a) the composite shell is made of a finite number of individually homogeneous layers,
b) the layers are perfectly bonded and no slip between them is possible,
c) the material is linearly elastic,
d) the shell is of moderate thickness enabling the application of the Equivalent Single Layer (ESL) model within the of First Order Shear Deformation (FOSD) Theory,
e) strains are small everywhere.

The above classic assumptions do not violate the salient geometric attributes of the considered 6-parameter shell theory i.e.:

f) translations and rotations are unlimited,
g) an arbitrary geometry of the shell reference surface is allowed, including folds, branches and intersections.

In the literature a number of approaches describing the multi-layer effect can be found, see for instance the review works[24],[25] or [26][26]. Since in this paper we are interested in the (structural) global response of the composite shell, we use the Equivalent Single Layer (ESL) model. The constitutive equations of the entire laminate are formulated for an equivalent single-layer panel endowed with macro-mechanical properties estimated as a weighted average of the mechanical properties of each lamina; see for instance [27]. However, if local effect are

to be considered (e.g. delamination), the layer-wise (e.g. [28] description must be used, see discussion for instance in [29]. Such problems are beyond the scope of the present paper.

2. OUTLINE OF FORMULATION

A rigorous mathematical derivation of the 6-parameter shell theory can be found in [2], [3], [4], [30] and will not be repeated here. In this section, for completeness, the main aspects of the underlying theory of shells are recalled in the range necessary for formulation of the constitutive relation.

In what follows the common convention of indices is adopted i.e. Latin indices run from 1 to 3 while Greek run from 1 to 2. Vectors are represented by boldface lower case characters while tensors by boldface capital letters. Comma indicates partial differentiation with respect to surface coordinates. Throughout it is assumed that all variables and domains are smooth enough to perform necessary mathematical operations.

The shell-like body is represented by the base surface M, not necessarily the middle surface, endowed with mechanical properties and an internal structure. To describe finite translations of such shell structure we use the translation vector field $\boldsymbol{u}(\boldsymbol{x}) = \boldsymbol{y}(\boldsymbol{x}) - \boldsymbol{x}$. Here $\boldsymbol{y}(\boldsymbol{x})$ denotes the position vector of the deformed base surface of the shell and $\boldsymbol{x}$ is the position vector of its initial configuration M, treated as the reference configuration. For the purpose of the present paper, we assume that M is formally parametrized by the orthogonal arc-length coordinates s_α with the associated unit vectors $\boldsymbol{t}^0_\beta = \boldsymbol{x}_{,\beta}$ locally tangent to M, and ~~a~~ the normal vector, $\boldsymbol{t}^0 \equiv \boldsymbol{t}^0_3 = \dfrac{\boldsymbol{t}^0_1 \times \boldsymbol{t}^0_2}{\| \boldsymbol{t}^0_1 \times \boldsymbol{t}^0_2 \|}$. In FEM implementation we assume that the vector $\boldsymbol{x}$ and the triad $\{\boldsymbol{t}^0_i\}$ are the input data of the problem. We take $\{\boldsymbol{t}^0_i\}$ as the rigid orthogonal frame i.e. $\boldsymbol{t}^0_i \cdot \boldsymbol{t}^0_j = \delta_{ij}$, $\boldsymbol{t}^0_i = \boldsymbol{t}^i_0$, $\boldsymbol{t}^0 \equiv \boldsymbol{t}^3_0$, $\| \boldsymbol{t}^0_i \| = 1$. Consequently, instead of a direct definition of the arc-length coordinates s_α as the input data we have the vectors $\{\boldsymbol{t}^0_i\}$ that determine the directions of s_α.

In the approach presented in the paper we do not need orthogonal arc-length coordinates directly but rather the tangent vectors. These vectors are included in the input data as the tensor $\boldsymbol{Q}(\boldsymbol{x})$. So the user decides how the $\boldsymbol{Q}(\boldsymbol{x})$ is oriented on each branch composing structural shell. It is a very simple and convenient way of modeling arbitrary orientable surfaces including irregular shells.

In each regular point of any branch composing irregular shell $\{\boldsymbol{t}^0_i\}$ is defined as a transformation of some global fixed base $\{\mathbf{e}_i\}$

$$\boldsymbol{t}^0_i(\boldsymbol{x}) = \boldsymbol{T}_0(\boldsymbol{x})\mathbf{e}_i, \quad \boldsymbol{T}_0 \in SO(3) \tag{1}$$

In view of the equation (1), any finite deformation of the directors is represented by the tensor field $\boldsymbol{Q}(\boldsymbol{x})$ (assumed as continuous over the entire domain of the irregular shell M) given by $\boldsymbol{t}_i(\boldsymbol{x}) = \boldsymbol{Q}(\boldsymbol{x})\boldsymbol{t}^0_i(\boldsymbol{x}) = \boldsymbol{Q}(\boldsymbol{x})\boldsymbol{T}_0(\boldsymbol{x})\mathbf{e}_i = \boldsymbol{T}(\boldsymbol{x})\mathbf{e}_i$, $\boldsymbol{Q}, \boldsymbol{T} \in SO(3)$. By using the relation (1), covariant components of the curvature tensor of M become

$$\mathrm{b}^0_{\alpha\beta} = -\boldsymbol{t}^0_{3,\beta} \cdot \boldsymbol{t}^0_\alpha = \boldsymbol{t}^0_{\alpha,\beta} \cdot \boldsymbol{t}^0 = (\boldsymbol{T}_0\mathbf{e}_i)_{,\beta} \cdot \boldsymbol{t}^0 = (\boldsymbol{T}_{0,\beta}\,\mathbf{e}_\alpha) \cdot \boldsymbol{t}^0 = (\boldsymbol{T}_{0,\beta}\,\boldsymbol{T}_0^T \boldsymbol{t}^0_\alpha) \cdot \boldsymbol{t}^0 \tag{2}$$

The components of the shifter tensor and its determinant, for any value of the thickness coordinate ζ (cf. Fig. 1), are

$$\mu_{\alpha\beta} = \delta_{\alpha\beta} - \zeta\, \mathrm{b}^0_{\alpha\beta}, \qquad \mu = \det \mu_{\alpha\beta} = 1 - 2\zeta H + \zeta^2 K,\ \zeta \in [-h^-, +h^+],\ h = h^+ + h^- \tag{3}$$

with $H = \frac{1}{2}(R_{min}^{-1} + R_{max}^{-1})$ being the mean curvature and $K = R_{min}^{-1} R_{max}^{-1}$ the Gaussian curvature of M. In view of Equation (3) the natural base vectors for any value $\zeta \in [-h^-, +h^+]$ are expressed as

$$\boldsymbol{g}^0_\alpha = \mu_{\alpha\beta} \boldsymbol{t}^0_\beta = (\delta_{\alpha\beta} - \zeta\, \mathrm{b}^0_{\alpha\beta}) \boldsymbol{t}^0_\beta \tag{4}$$

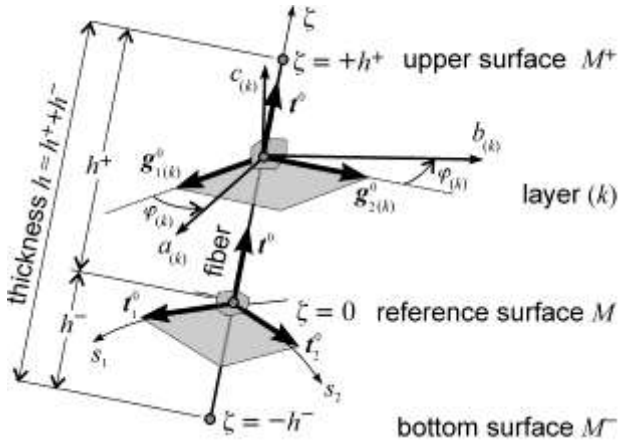

Fig. 1. Local shell coordinate systems

In the following derivations the local parametrization of rotations is based on the application of the finite rotation vector $\boldsymbol{w}$ in the spatial representation; however, the presented formulation, in general, is independent of any chosen parametrization. The tensor $\boldsymbol{Q} \in SO(3)$ in the canonical parametrization assumes the form $\boldsymbol{Q} = \mathbf{1} + a\boldsymbol{W} + b\boldsymbol{W}^2$, where $\boldsymbol{W} = \mathrm{ad}(\boldsymbol{w}) \in so(3)$, $a = \dfrac{\sin w}{w}$, $b = \dfrac{1 - \cos w}{w^2}$, $w = \sqrt{\boldsymbol{w} \cdot \boldsymbol{w}}$ and the operator $\mathrm{ad}^{-1}(.)$ takes the axial vector out of the skew tensor. The vectorial strain measures and their virtual counterparts (cf. [1], [2], [3], [4]) are:

- the stretching vector

$$\boldsymbol{\varepsilon}_\beta = \boldsymbol{y}_{,\beta} - \boldsymbol{t}_\beta = \boldsymbol{u}_{,\beta} + (\mathbf{1} - \boldsymbol{Q})\boldsymbol{t}^0_\beta, \quad \delta\boldsymbol{\varepsilon}_\beta = \boldsymbol{v}_{,\beta} + \boldsymbol{y}_{,\beta} \times \boldsymbol{w} \tag{5}$$

- the bending vector

$$\boldsymbol{\kappa}_\beta = \mathrm{ad}^{-1}(\boldsymbol{Q}_{,\beta} \boldsymbol{Q}^{\mathrm{T}}), \qquad \delta\boldsymbol{\kappa}_\beta = \boldsymbol{w}_{,\beta} \tag{6}$$

When expressed in a weak form, the boundary value problem for a layered shell structure is stated as follows. Given the external resultant force and couple vector fields $\boldsymbol{f}(\boldsymbol{x})$ and $\boldsymbol{c}(\boldsymbol{x})$ on $\boldsymbol{x} \in M$, $\boldsymbol{n}^*(\boldsymbol{x})$ and $\boldsymbol{m}^*(\boldsymbol{x})$ along ∂M_f, the kinematic boundary conditions $\boldsymbol{u}(\boldsymbol{x}) = \boldsymbol{u}^*(\boldsymbol{x})$ and $\boldsymbol{Q}(\boldsymbol{x}) = \boldsymbol{Q}^*(\boldsymbol{x})$ along $\partial M_d = \partial M \setminus \partial M_f$, find a curve $\mathbf{u}(\boldsymbol{x}) = (\boldsymbol{u}(\boldsymbol{x}), \boldsymbol{Q}(\boldsymbol{x}))$ on the configuration space $C(M, E^3 \times SO(3))$ such that for any continuous kinematically admissible virtual vector field $\mathbf{w}(\boldsymbol{x}) \equiv (\boldsymbol{v}(\boldsymbol{x}), \boldsymbol{w}(\boldsymbol{x}))$ the following principle of virtual work (PVW) is satisfied:

$$G[\mathbf{u}; \mathbf{w}] = \int\!\!\int_M [\boldsymbol{n}^\beta \cdot (\boldsymbol{v}_{,\beta} + \boldsymbol{y}_{,\beta} \times \boldsymbol{w}) + \boldsymbol{m}^\beta \cdot \boldsymbol{w}_{,\beta}]\, da - \int\!\!\int_M (\boldsymbol{f} \cdot \boldsymbol{v} + \boldsymbol{c} \cdot \boldsymbol{w})\, da - \int_{\partial M_f} (\boldsymbol{n}^* \cdot \boldsymbol{v} + \boldsymbol{m}^* \cdot \boldsymbol{w}) ds = 0\,. \tag{7}$$

In above equation, it is implicitly assumed that the virtual vector fields are kinematically admissible if $\boldsymbol{v}(\boldsymbol{x})=\boldsymbol{0}$ and $\boldsymbol{w}(\boldsymbol{x})=\boldsymbol{0}$ along ∂M_d.

For the completeness of the exposition we present respectively the decompositions of $\boldsymbol{\varepsilon}_\beta$ and $\boldsymbol{\kappa}_\beta$ from (5) and (6) and $\boldsymbol{n}^\beta$ and $\boldsymbol{m}^\beta$ from (7) i.e.

$$\begin{aligned} \boldsymbol{\varepsilon}_\beta &= \varepsilon_{\beta 1}\boldsymbol{t}_1+\varepsilon_{\beta 2}\boldsymbol{t}_2+\varepsilon_\beta \boldsymbol{t}_3 & \boldsymbol{n}^\beta &= N^{\beta 1}\boldsymbol{t}_1+N^{\beta 2}\boldsymbol{t}_2+Q^\beta \boldsymbol{t}_3 \\ \boldsymbol{\kappa}_\beta &= \boldsymbol{t}\times(\kappa_{\beta 1}\boldsymbol{t}_1+\kappa_{\beta 2}\boldsymbol{t}_2)+\kappa_\beta \boldsymbol{t}_3 \,, & \boldsymbol{m}^\beta &= \boldsymbol{t}\times(M^{\beta 1}\boldsymbol{t}_1+M^{\beta 2}\boldsymbol{t}_2)+M^\beta \boldsymbol{t}_3 \end{aligned} \tag{8}$$

A numerical solution of Eq. (7)(7) can be obtained in the course of an iterative procedure reducing the problem to a sequence of solutions of linearized problems. Each linearized problem is formulated at discrete values of the spatial variables (FEM). The presence of $SO(3)$ group in the definition of the configuration space $C(M, E^3\times SO(3))$ causes the main difficulty of such a solution procedure.

The strain components introduced in (5)(5)-(6)-(6) are collected in the vector $\boldsymbol{\varepsilon}$ (spatial representation)

$$\boldsymbol{\varepsilon}=\{\varepsilon_{11}\ \varepsilon_{22}\ \varepsilon_{12}\ \varepsilon_{21}|\varepsilon_1\ \varepsilon_2\|\kappa_{11}\ \kappa_{22}\ \kappa_{12}\ \kappa_{21}|\kappa_1\ \kappa_2\}^T=\{\boldsymbol{\varepsilon}_m|\boldsymbol{\varepsilon}_s\|\boldsymbol{\varepsilon}_b|\boldsymbol{\varepsilon}_d\}^T \tag{9}$$

where labels m, s, b, d denote respectively: the membrane, shear, bending and drilling parts. To Eq. (9) we adjoin the vector of shell stress and couple resultants

$$\mathbf{s}=\{N^{11}N^{22}N^{12}N^{21}|Q^1Q^2\|M^{11}M^{22}M^{12}M^{21}|M^1M^2\}^T=\{\mathbf{s}_m|\mathbf{s}_s\|\mathbf{s}_b|\mathbf{s}_d\}^T \tag{10}$$

through the constitutive equation

$$\mathbf{s}=\mathbf{C}\boldsymbol{\varepsilon} \tag{11}$$

The explicit form of $\mathbf{C}$, which is the main goal of the present paper, and definitions of the shell resultants are presented in Section 3.

In the relations (9) and (10), the respective components of membrane and bending strain measures are not symmetric, which is a direct consequence of the implementation of the statically and kinematically exact Cosserat type shell theory. Asymmetric strain and stress measures appear in theories that take into account the microstructure of the body, see for instance [31], [32], [33].

Let us apply a spatial approximation to the PVW Eq. (7). The base surface of the shell M is approximated as a sum $M\approx M_h=\sum_{e=1}^{N_e}\Pi_{(e)}$, where N_e is the number of finite elements. A typical finite element $\Pi_{(e)}$ is defined as a smooth image of the so-called standard element $\pi_{(e)}$. Here $\pi_{(e)}=[-1,+1]\times[-1,+1]$ is the element in the parent (natural) domain $\boldsymbol{\xi}=(\xi_1,\xi_2)$. Within N - node element vector-type variables are interpolated using the standard direct Lagrange-type interpolation rule

$$\boldsymbol{x}(\boldsymbol{\xi})=\sum\nolimits_{a=1}^{N}L_a(\boldsymbol{\xi})\,\boldsymbol{x}_a \tag{12}$$

The vector of virtual rotations $\boldsymbol{w}(\boldsymbol{\xi})$ is interpolated here in the fixed frame $\{\mathbf{e}_i\}$, since in the general case of structural shells (even in a case of regular but curved shells) the base $\{\boldsymbol{t}_i(\boldsymbol{x})\}$ varies in space from point to point on M. Hence interpolation in the local shell base $\{\boldsymbol{t}_i(\boldsymbol{x})\}$ (that can be found in the literature on 5-parameter shell theory or on rod/beam elements) is not entirely correct. By making use of the relation

$$\boldsymbol{w}(\xi) = w_i(\xi)\,\boldsymbol{t}_i(\xi) = \bar{w}_j(\xi)\,\mathbf{e}_j = \bar{w}_j(\xi)\,\boldsymbol{T}^T(\xi)\,\boldsymbol{t}_j(\xi) = T_{ji}(\xi)\,\bar{w}_j(\xi)\,\boldsymbol{t}_i(\xi) \tag{13}$$

we employ the following interpolating scheme

$$\boldsymbol{w}(\xi) = \begin{Bmatrix} w_1(\xi) \\ w_2(\xi) \\ w_3(\xi) \end{Bmatrix} = \mathbf{T}^T(\xi)\bar{\boldsymbol{w}}(\xi), \qquad \bar{\boldsymbol{w}}(\xi) = \begin{Bmatrix} \bar{w}_1(\xi) \\ \bar{w}_2(\xi) \\ \bar{w}_3(\xi) \end{Bmatrix} = \sum_{a=1}^{N} L_a(\xi) \begin{Bmatrix} \bar{w}_{1a} \\ \bar{w}_{1a} \\ \bar{w}_{1a} \end{Bmatrix}, \qquad \xi \in \pi_{(e)} \tag{14}$$

To evaluate Eq. (14) it is necessary to interpolate the matrix $\mathbf{T}(\xi) = [T_{ij}]$ as a result of a superposition of the rotation tensors $\boldsymbol{T}(\xi) = \boldsymbol{Q}(\xi)\boldsymbol{T}_0(\xi) \Rightarrow \{\boldsymbol{t}_i(\xi)\}$ according to the scheme appropriate for $SO(3)$-valued functions, so that $\mathbf{T}(\xi) \in SO(3) \;\; \forall \xi \in \pi_{(e)}$. Such an interpolation was originally proposed in [2] while the variant used here has been worked out in [34] (in Polish) and in [35] (in English), cf. also [4]. Some details of such an interpolation on $SO(3)$ are recollected in Appendix 1.

3. MATERIAL LAW

In section 2 we have summarized the statically and kinematically exact parts of the present formulation of shell theory. The spatial approximation is consistent with the FEM approach. Here we discuss corresponding constitutive equations which, being the physical laws, are always subjected to some experimental errors.

As indicated above, the underlying kinematic model of the presented shell theory is formally equivalent to that of the 2D Cosserat surface. Material law for an isotropic Cosserat (or micropolar) continuum has been discussed among others in [31], [32], [33], [36] or [37]. In a 2D continuum problem four material constants are necessary to properly describe isotropy, see for instance [37] or [38]. The values of these constants for different materials, either in a three dimensional case or in a two dimensional one, result from symmetry considerations [39] and experimental studies, see for example [40] or [41] and references given there.

In the present context of a transversely orthotropic shell, the use of 3D orthotropic linearly elastic Cosserat continuum would be the most appropriate choice. The material law of such a 3D continuum was discussed among others in, [42], [43], [44], [45]. Micropolar material that is orthotropic for both force stress and couple stress requires nine elastic constants in a two dimensional case, cf. [43]. Some methods of identifying these constants can be found for instance in, [43], [44]. In particular, in [43] an interesting route from five elastic constants of classical anisotropic material to nine constants of orthotropic Cosserat medium has been shown.

In this paper we assume a different train of reasoning. We propose the material law for the composite Cosserat shell as following directly from the constitutive relation for a 2D nonpolar orthotropic linearly elastic continuum. This intuitive methodology allows us to use five material constants of the classical elastic continuum with one additional parameter on the 2D level as the torsional factor already discussed in [2], [3], [4].

This approach is justified by the fact that the results presented in the majority of papers concerned with composite shells have been obtained assuming 3D constitutive relations of a Cauchy continuum. Thus, applying our constitutive equations we are able to perform a direct comparison of results. The problem of identifying the elastic constants for a Cosserat-type shell is beyond the scope of the present paper.

3.1. FORMULATION ON LAYER LEVEL

We assume that each lamina is made of a linearly elastic transversely isotropic material. An orthogonal system of material axes $(a_{(k)}, b_{(k)}, c_{(k)})$ is introduced in each lamina (k), as shown in **Fig. 2**. These axes define a local triad such that the $a_{(k)}$ -axis is aligned with a possible reinforcement and the $c_{(k)}$ -axis is locally normal to the layer reference surface in the shell.

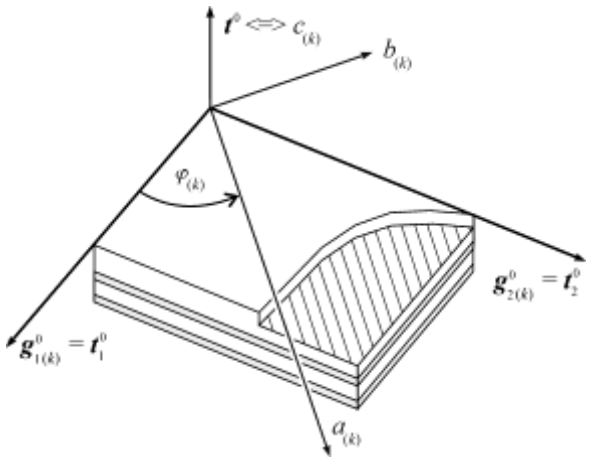

Fig. 2. Local layer (k) system of material axes for the flat shell of constant thickness

Taking into account the assumptions of the FOSD type theory (see for instance [26], [46]) for material only, and in order to avoid the discussion about the influence of shell deformation in the transverse normal direction, we assume the plane stress state in each layer. We formulate the following simplest generalization (here written in terms of physical components) of the constitutive relation for the in-plane stress (omitting the symmetry condition) and the transverse shear components in the k th layer:

$$\begin{Bmatrix} \sigma_{aa} \\ \sigma_{bb} \\ \sigma_{ab} \\ \sigma_{ba} \\ \hline \sigma_a \\ \sigma_b \end{Bmatrix}_k = \left[\begin{array}{cccc|cc} \frac{E_a}{1-\nu_{ab}\nu_{ba}} & \frac{\nu_{ab}E_b}{1-\nu_{ab}\nu_{ba}} & 0 & 0 & 0 & 0 \\ \frac{\nu_{ba}E_a}{1-\nu_{ab}\nu_{ba}} & \frac{E_b}{1-\nu_{ab}\nu_{ba}} & 0 & 0 & 0 & 0 \\ 0 & 0 & 2G_{ab} & 0 & 0 & 0 \\ 0 & 0 & 0 & 2G_{ab} & 0 & 0 \\ \hline 0 & 0 & 0 & 0 & 2G_{ac} & 0 \\ 0 & 0 & 0 & 0 & 0 & 2G_{bc} \end{array}\right]_k \begin{Bmatrix} \varepsilon^{aa} \\ \varepsilon^{bb} \\ \varepsilon^{ab} \\ \varepsilon^{ba} \\ \hline \varepsilon^{a} \\ \varepsilon^{b} \end{Bmatrix}_k \tag{15}$$

$$\begin{Bmatrix} \boldsymbol{\sigma}^{mat}_m \\ \hline \boldsymbol{\sigma}^{mat}_s \end{Bmatrix}_k = \left[\begin{array}{c|c} \tilde{\boldsymbol{C}}_m & \boldsymbol{0}_{4\times 2} \\ \hline \boldsymbol{0}_{4\times 2} & \tilde{\boldsymbol{C}}_s \end{array}\right]_k \begin{Bmatrix} \boldsymbol{\varepsilon}^{mat}_m \\ \hline \boldsymbol{\varepsilon}^{mat}_s \end{Bmatrix}_k = \tilde{\boldsymbol{C}}_k \begin{Bmatrix} \boldsymbol{\varepsilon}^{mat}_m \\ \hline \boldsymbol{\varepsilon}^{mat}_s \end{Bmatrix}_k \tag{16}$$

expressed in terms of: $(E_a)_k$, $(E_b)_k$ - Young's moduli in the direction of the reinforcement and perpendicularly to the reinforcement, respectively, $(G_{ab})_k$ - shear modulus in $a-b$ plane, $(\nu_{ab})_k$, $(\nu_{ba})_k$ - Poisson's ratios such that $E_a\nu_{ba} = E_b\nu_{ab}$ (no summation). Denoting by $\varphi_{(k)}$ the angle between the local $a_{(k)}$ axis and $\boldsymbol{g}^0_{1(k)}$ vector, with the abridged notation $C = \cos(\varphi_{(k)})$ and $S = \sin(\varphi_{(k)})$, transformation of the stress and strain vectors between the material axes and $\{\boldsymbol{g}^0_\alpha\}_k$ can be expressed by the following relations:

$$\left\{\begin{matrix}\boldsymbol{\sigma}_m^{mat}\\ \boldsymbol{\sigma}_s^{mat}\end{matrix}\right\}_k=\left[\begin{array}{c|c}\tilde{\mathbf{T}}_m & \mathbf{0}_{4\times 2}\\ \hline \mathbf{0}_{2\times 4} & \tilde{\mathbf{T}}_s\end{array}\right]_k\left\{\begin{matrix}\boldsymbol{\sigma}_m\\ \boldsymbol{\sigma}_s\end{matrix}\right\}_k=\tilde{\mathbf{T}}_k\left\{\begin{matrix}\boldsymbol{\sigma}_m\\ \boldsymbol{\sigma}_s\end{matrix}\right\}_k,\qquad \left\{\begin{matrix}\boldsymbol{\varepsilon}_m^{mat}\\ \boldsymbol{\varepsilon}_s^{mat}\end{matrix}\right\}\left[\begin{array}{c|c}\tilde{\mathbf{T}}_m & \mathbf{0}_{4\times 2}\\ \hline \mathbf{0}_{2\times 4} & \tilde{\mathbf{T}}_s\end{array}\right]\left\{\begin{matrix}\boldsymbol{\varepsilon}_m\\ \boldsymbol{\varepsilon}_s\end{matrix}\right\}=\tilde{\mathbf{T}}\left\{\begin{matrix}\boldsymbol{\varepsilon}_m\\ \boldsymbol{\varepsilon}_s\end{matrix}\right\} \tag{17}$$

with transformation matrix defined as

$$\tilde{\mathbf{T}}_k=\left[\begin{array}{cccc|cc}C^2 & S^2 & SC & SC & 0 & 0\\ S^2 & C^2 & -SC & -SC & 0 & 0\\ -SC & SC & C^2 & -S^2 & 0 & 0\\ -SC & SC & -S^2 & C^2 & 0 & 0\\ \hline 0 & 0 & 0 & 0 & C & -S\\ 0 & 0 & 0 & 0 & S & C\end{array}\right]_k=\left[\begin{array}{c|c}\tilde{\mathbf{T}}_m & \mathbf{0}_{4\times 2}\\ \hline \mathbf{0}_{2\times 4} & \tilde{\mathbf{T}}_s\end{array}\right]_k, \tag{18}$$

Therefore, the constitutive matrix follows in the form

$$\left\{\begin{matrix}\boldsymbol{\sigma}_m\\ \boldsymbol{\sigma}_s\end{matrix}\right\}_k=\left[\begin{array}{c|c}\tilde{\mathbf{T}}_m^{-1}\tilde{\boldsymbol{C}}_m\tilde{\mathbf{T}}_m & \mathbf{0}_{4\times 2}\\ \hline \mathbf{0}_{4\times 2} & \tilde{\mathbf{T}}_s^{-1}\tilde{\boldsymbol{C}}_s\tilde{\mathbf{T}}_s\end{array}\right]_k\left\{\begin{matrix}\boldsymbol{\varepsilon}_m\\ \boldsymbol{\varepsilon}_s\end{matrix}\right\}_k=\left[\begin{array}{c|c}\boldsymbol{C}_m & \mathbf{0}_{4\times 2}\\ \hline \mathbf{0}_{4\times 2} & \boldsymbol{C}_s\end{array}\right]_k\left\{\begin{matrix}\boldsymbol{\varepsilon}_m\\ \boldsymbol{\varepsilon}_s\end{matrix}\right\}_k \tag{19}$$

3.2. STRESS AND COUPLE RESULTANT FORMULATION

The discussion of the constitutive equations given below is divided into two parts. In the first part we express the membrane $\mathbf{s}_m$, shear $\mathbf{s}_s$ and bending $\mathbf{s}_b$ resultants Eq. (10) in terms of corresponding stresses Eq. (19). The derivation follows standard steps for a Mindlin-Reissner type shell theory. In the second part we deal with the drilling resultants $\mathbf{s}_d$.

The stress and couple resultants Eq. (10) are formally defined as integrals over the shell thickness $h=h^+ + h^-$ from appropriate stresses. Integration taking into account the shell curvature formally reads $\iiint_V(\cdots)\,\mathrm{d}v=\iint_A\left(\int_{-h^-}^{+h^+}(\cdots)\,\mu\,d\zeta\right)da$, $\zeta\in[-h^-,+h^+]$ with μ given by Eq. (3). Assuming that the laminate in question consists of N_L layers, each of the thickness $h_k=\zeta_k^+-\zeta_k^-$, where ζ_k^+ and ζ_k^- denote respectively the distance from the reference surface to the top and bottom of the k^{th} layer (for shells with a solid core $\zeta_k^-\equiv\zeta_{k-1}^+$, $\zeta_{k+1}^-\equiv\zeta_k^+$ where $\zeta_0^+=-h^-$, $\zeta_{N_L}^+=+h^+$) and using Eq. (9) and Eq. (10) we write

$$\mathbf{s}_m=\int_{-h^-}^{+h^+}\boldsymbol{\sigma}_m\,\mu\,d\zeta=\sum_{k=1}^{N_L}\left(\int_{\zeta_k^-}^{\zeta_k^+}\{\boldsymbol{\sigma}_m\}_k\,\mu\,d\zeta\right),\qquad \zeta\in[\zeta_k^-;\zeta_k^+] \tag{20}$$

$$\mathbf{s}_s=\int_{-h^-}^{+h^+}\boldsymbol{\sigma}_s\,\mu\,d\zeta=\sum_{k=1}^{N_L}\left(\int_{\zeta_k^-}^{\zeta_k^+}\{\boldsymbol{\sigma}_s\}_k\,\mu\,d\zeta\right) \tag{21}$$

$$\mathbf{s}_b=\int_{-h^-}^{+h^+}\boldsymbol{\sigma}_m\,\zeta\,\mu\,d\zeta=\sum_{k=1}^{N_L}\left(\int_{\zeta_k^-}^{\zeta_k^+}\{\boldsymbol{\sigma}_m\}_k\,\zeta\,\mu\,d\zeta\right) \tag{22}$$

By taking into account the assumption of a FOSD type theory (see for instance [26]-or [46]) the above relations can be rewritten as

$$\mathbf{s}_m=\sum_{k=1}^{N_L}\left(\int_{\zeta_k^-}^{\zeta_k^+}\{\boldsymbol{C}_m\}_k\left(\boldsymbol{\varepsilon}_m+\zeta\boldsymbol{\varepsilon}_b\right)\mu\,d\zeta\right)=\underset{4\times 4}{\mathbf{A}}\,\boldsymbol{\varepsilon}_m+\underset{4\times 4}{\mathbf{B}}\,\boldsymbol{\varepsilon}_b \tag{23}$$

$$\mathbf{s}_s = \sum_{k=1}^{N_L}\left(\int_{\zeta_k^-}^{\zeta_k^+}(\alpha_s)_k\{\boldsymbol{C}_s\}_k\,\boldsymbol{\varepsilon}_s\,\mu\,d\zeta\right) = \underset{2\times 2}{\mathbf{S}}\,\boldsymbol{\varepsilon}_s \tag{24}$$

$$\mathbf{s}_b = \sum_{k=1}^{N_L}\left(\int_{\zeta_k^-}^{\zeta_k^+}\{\boldsymbol{C}_m\}_k\left(\zeta\,\boldsymbol{\varepsilon}_m + (\zeta)^2\boldsymbol{\varepsilon}_b\right)\mu\,d\zeta\right) = \underset{4\times 4}{\mathbf{B}}\,\boldsymbol{\varepsilon}_m + \underset{4\times 4}{\mathbf{D}}\,\boldsymbol{\varepsilon}_b \tag{25}$$

where $(\alpha_s)_k$ is the shear correction factor of the k^{th} layer. Usually, it is assumed that the approximation $\mu \approx 1$ holds. This assumption is justifiable for thin shells ($h \ll L$, L - a typical dimension, with a small curvature $h \ll R_{min}$ see Eq. (3)). Assuming that $\mu \approx 1$, the matrices in Eqs. (23)-(25) are defined as

$$\underset{4\times 4}{\mathbf{A}} = \sum_{k=1}^{N_L}\{\boldsymbol{C}_m\}_k\left(\zeta_k^+ - \zeta_k^-\right), \qquad \underset{4\times 4}{\mathbf{B}} = \tfrac{1}{2}\sum_{k=1}^{N_L}\{\boldsymbol{C}_m\}_k\left((\zeta_k^+)^2 - (\zeta_k^-)^2\right) \tag{26}$$

$$\underset{4\times 4}{\mathbf{D}} = \tfrac{1}{3}\sum_{k=1}^{N_L}\{\boldsymbol{C}_m\}_k\left((\zeta_k^+)^3 - (\zeta_k^-)^3\right), \qquad \underset{2\times 2}{\mathbf{S}} = \sum_{k=1}^{N_L}(\alpha_s)_k\{\boldsymbol{C}_s\}_k\left(\zeta_k^+ - \zeta_k^-\right) \tag{27}$$

For the drilling couples we formally write

$$\mathbf{s}_d = \int_{-h^-}^{+h^+}\boldsymbol{\sigma}_d\,\mu\,d\zeta = \sum_{k=1}^{N_L}\left(\int_{\zeta_k^-}^{\zeta_k^+}\{\boldsymbol{\sigma}_d\}_k\,\mu\,d\zeta\right) \tag{28}$$

Notation in (28) is a purely formal one because we do not use couple-stress $\boldsymbol{\sigma}_d$ on the layer level. Instead, in this paper, we propose to express the resultant drilling stresses $\mathbf{s}_d$ in terms of the drilling strains $\boldsymbol{\varepsilon}_d$ through

$$\mathbf{s}_d = \alpha_t\sum_{k=1}^{N_L}\left(\int_{\zeta_k^-}^{\zeta_k^+}(\alpha_t)_k\{\boldsymbol{C}_d\}_k\,\boldsymbol{\varepsilon}_d\,\mu\,d\zeta\right) = \underset{2\times 2}{\mathbf{G}}\,\boldsymbol{\varepsilon}_d\,, \quad \boldsymbol{C}_d = \zeta^2\boldsymbol{C}_s \tag{29}$$

with $\boldsymbol{C}_s$ given in Eq. (19). The term ζ^2 in Eq. $(29)_2$ is introduced to keep the dimension consistency and, in the limit passage to homogenous isotropic shells, to ensure the compatibility with previous propositions, cf. [1], [2], [3], [4]. The material constant $(\alpha_t)_k$ (not to be mistaken with a penalty parameter) is the torsional factor of the k^{th} layer, viewed as an analogue of the shear factor α_s, (cf. relation (24)) - a material coefficient established for the present theory of shells. The value of α_t and its definition are still an open problems in the context of the 6-parameter theory of shells. This issue has been extensively investigated in [2]-[3]. The studies and numerical simulations for $\alpha_t \in [10^{-10}, 10^{+10}]$ carried out there revealed that values of α_t from 0 up to 1 have a negligible influence on the values of displacements and on the internal energy of the shell structure. For numerical simulations presented in this paper, it was assumed $\alpha_t = 0.01$ together with $(\alpha_t)_k = 1$. Therefore for the drilling resultants we have

$$\underset{2\times 2}{\mathbf{G}} = \tfrac{1}{3}\sum_{k=1}^{N_L}(\alpha_t)_k\{\boldsymbol{C}_s\}_k\left((\zeta_k^+)^3 - (\zeta_k^-)^3\right) \tag{30}$$

Summarizing, the constitutive equation (11) for the composite shell used here takes the following form

$$\underset{12\times 1}{\begin{Bmatrix}\mathbf{s}_m\\ \mathbf{s}_s\\ \mathbf{s}_b\\ \mathbf{s}_d\end{Bmatrix}} = \underset{12\times 12}{\begin{bmatrix}\underset{4\times 4}{\mathbf{A}} & \mathbf{0} & \underset{4\times 4}{\mathbf{B}} & \mathbf{0}\\ \mathbf{0} & \underset{2\times 2}{\mathbf{S}} & \mathbf{0} & \mathbf{0}\\ \underset{4\times 4}{\mathbf{B}} & \mathbf{0} & \underset{4\times 4}{\mathbf{D}} & \mathbf{0}\\ \mathbf{0} & \mathbf{0} & \mathbf{0} & \underset{2\times 2}{\mathbf{G}}\end{bmatrix}}\underset{12\times 1}{\begin{Bmatrix}\boldsymbol{\varepsilon}_m\\ \boldsymbol{\varepsilon}_s\\ \boldsymbol{\varepsilon}_b\\ \boldsymbol{\varepsilon}_d\end{Bmatrix}} \tag{31}$$

Here all the submatrices are functions of five engineering material constants of orthotropic material with an additional dependence of $\mathbf{G}$ on the sixth parameter α_t whose value has been assumed based on numerical computations.

In passing, we note that the constitutive relation (11) for homogenous isotropic shells has been discussed in e.g. [1], [2], [3], [4].

4. EXAMPLES

Below we analyze some representative examples validating the presented approach. The present report focuses primarily on a geometrically non-linear analysis of problems involving large displacements and rotations with orthotropic and homogenous isotropic elastic materials. The strength of the present formulation to analyze irregular shell structures with folds is underlined by solving two examples.

In computations we use fine meshes of 16-node CAM elements (denoted as CAMe16) with full integration (FI) and regular node distribution. Thereby we avoid discussions about a mesh convergence, spurious zero-energy forms or the satisfaction of a patch-test. In the latter case we refer to [47] for important results concerning the satisfaction of an out-of-plane bending patch-test for low order elements. Moreover, such discretization is able to represent complicated and compound deformation waves that may appear during the deformation. In all examples the orientation of material axes is described with respect to the director $\boldsymbol{g}^0_{1(k)} \equiv \boldsymbol{t}^0_1$. The convergence check is performed by using the selective relative criteria. The criteria are imposed on norms of increments (corrections) $\delta(\Delta \boldsymbol{u})$ generated through equilibrium iterations. In symbolic notation the above criteria may be written as $\dfrac{\| \delta(\Delta \boldsymbol{u}) \|}{\| \Delta \boldsymbol{u} \|} < 0.001$, $\dfrac{\max\limits_i | \delta(\Delta u_i) |}{\max\limits_i | \Delta u_i |} < 0.01$.

4.1. Semi-cylindrical shell under point load.

This is one of the most demanding benchmark tests for large rotation shell analysis – see Fig. 3. This example was introduced by Stander et al. [48]. The case of a layered composite shell was examined among others in [49], [50], [51]. We assume two different cross-ply lamination schemes: [90/0/90] and [0/90/0] and the following dimensions: $L = 304.8$ mm, $R = 101.6$ mm $h = 3$ mm; together with material parameters for boron-epoxy type composites: $E_a = 20.685$ kN/mm^2, $E_b = 5.17125$ kN/mm^2, $G_{ab} = G_{ac} = 7.956$ kN/mm^2, $G_{bc} = 1.989$ kN/mm^2 and $\nu_{ab} = 0.25$. For the homogenous isotropic case the following material properties are used: $E = 20.685$ kN/mm^2, $\nu = 0.25$. The load is assumed to be proportional: $P(\lambda) = \lambda P_{ref}$, where $P_{ref} = 1000$ kN. The results obtained using 40×40 CAMe16(FI) elements are depicted in Fig. 3. The graphs show very good agreement with the reference solution [50].

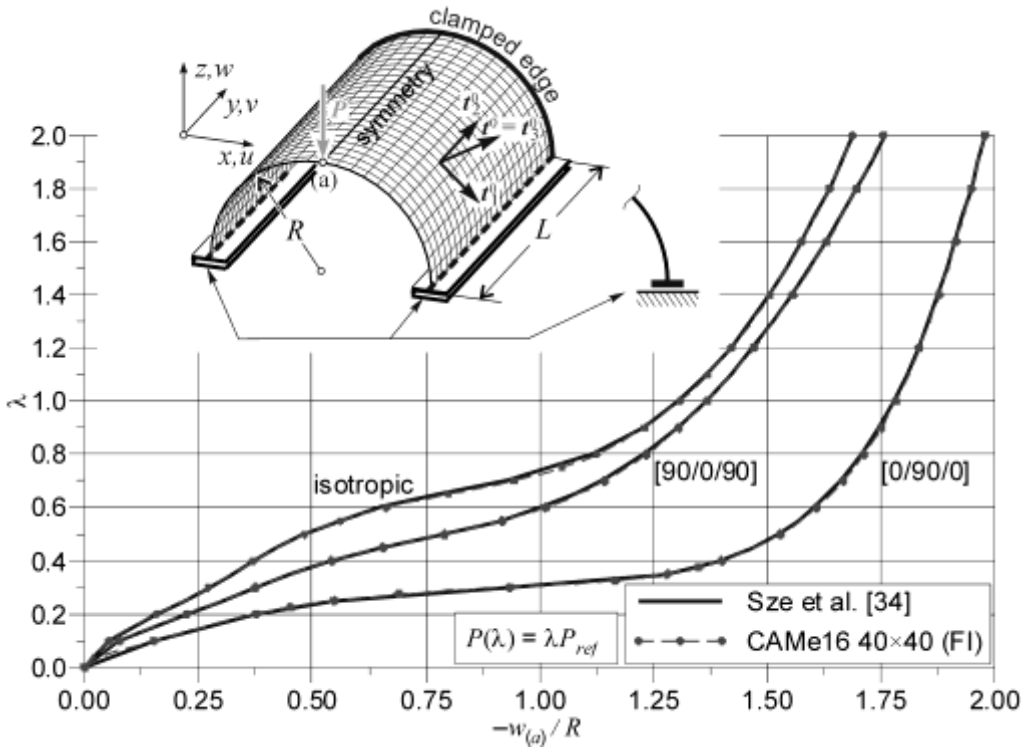

Fig. 3. Semi-cylindrical shell under a point load, geometry and results

4.2. Two layer cross-ply [0/90] *simply supported spherical shell*

As the second example we consider the popular problem (see, for instance [52], [53]) of a simply supported spherical shell under uniform inward pressure. Here we analyze the variant proposed in [22]. The shell from Fig. 4 is cut by four vertical planes acting on a sphere having radius $R = 1000$ in. The rectangular projection of the edges forms a $2L \times 2L$ square, $L = 50$ in. Two layers $h = 0.5$ in each are taken, made of the same orthotropic material but with different ply orientations. The lamination sequence designated as [0/90] means that the material axes of the bottom layer coincide with the axes of the shell coordinate system. The material properties of the lamina are: $E_1 = 25 \times 10^6$ psi, $E_2 = 10^6$ psi, $G_{12} = G_{13} = 5 \times 10^5$ psi, $G_{23} = 2 \times 10^5$ psi, $\nu_{12} = 0.25$. We analyze two variants (BC1 and BC3) of simply supported boundary conditions as in [22] . Fig. 4 depicts the comparison of results. The graph shows a quite good agreement with the reference solution [22].

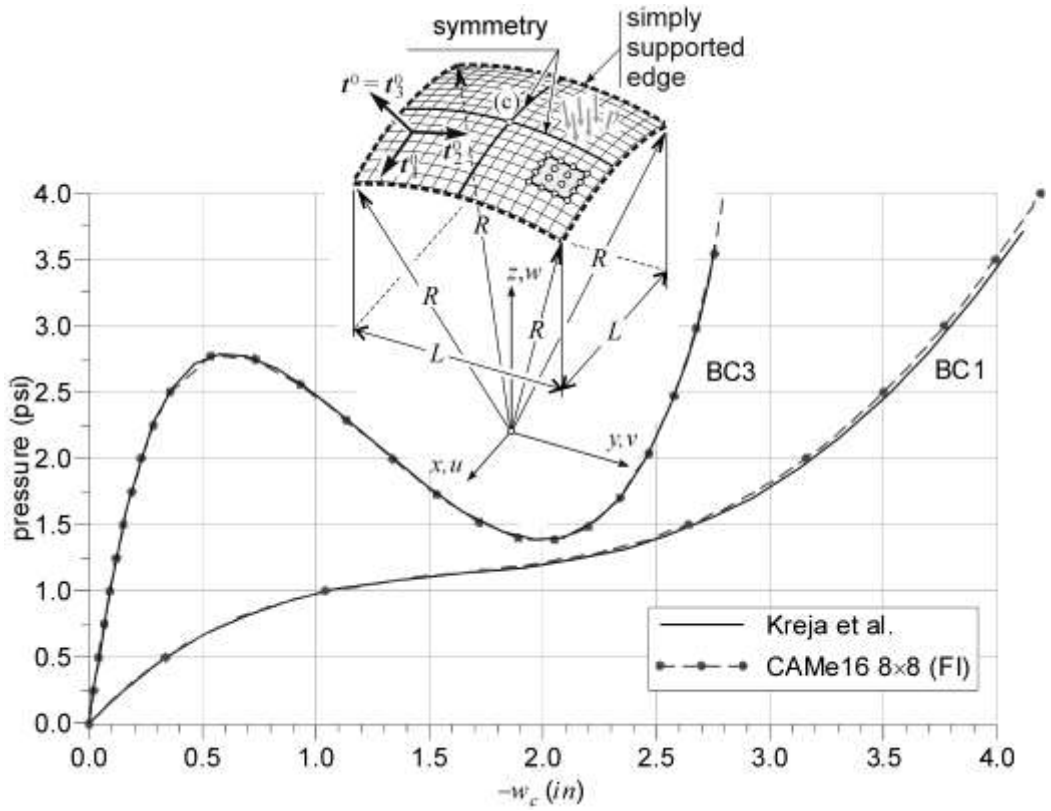

Fig. 4. Simply supported spherical shell, geometry and results

4.3. Three layer hyperboloid shell

We examine the well-known example of hyperboloid shell under action of two opposite point forces. Due to symmetries only an octant of the shell is analyzed – see Fig. 5. This demanding large displacement and rotations problem can be traced back to [28] and it is popular ever since (see for instance [47], [51], [55], [56]). Bathe and his co-workers, see for instance [57] or [58] and references given therein, studied in-depth a similar example, but as a homogenous isotropic problem, pointing out important results concerning, among others, various sources of locking. The geometry, load and material properties used in the present paper are: $h = 0.04$ m, $R_1 = 7.5$ m, $R_2 = 15$ m, $H = 20.0$ m, $R(y) = R_1\sqrt{1+(y/C)^2}$, $C = 20/\sqrt{3}$, $P(\lambda) = \lambda P_{ref}$, $P_{ref} = 5$ kN, $E_1 = 40\times10^6$ kN/m^2, $E_2 = 10^6$ kN/m^2, $G_{12} = G_{13} = G_{23} = 0.6\times10^6$ kN/m^2, $\nu_{12} = 0.25$.

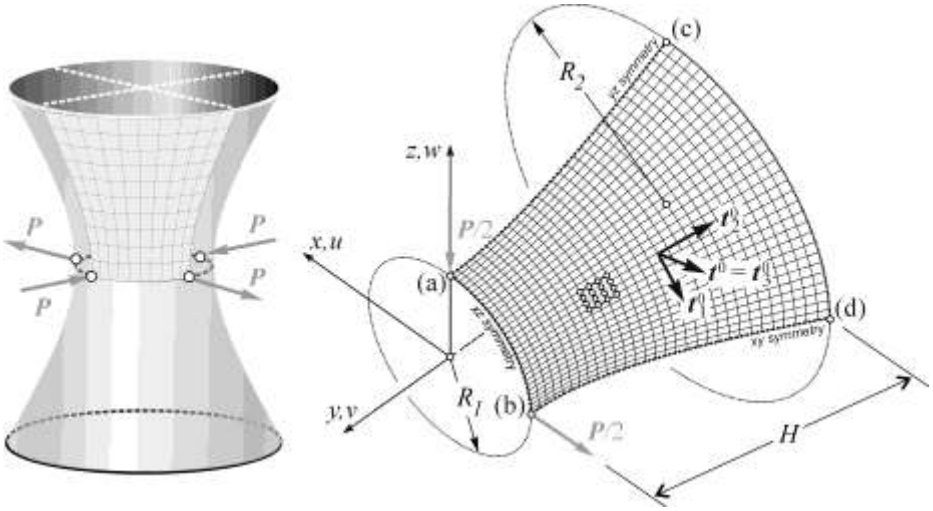

Fig. 5. Hyperboloid shell, geometry

The obtained results are depicted in Fig. 6 and in Fig. 7. For the lamination [0/90/0] our results are in a very good agreement with the reference solution. In the second laminate layout [90/0/90] the solutions are in agreement up to the load multiplier $\lambda = 15$. Above this value significant discrepancies are observed. Some preliminary results based on the discussed formulation indicate that the discrepancies may be attributed to a poor mesh density used in [28]. This observation has motivated our further nonlinear convergence analysis, carried out for values of the load multiplier significantly larger than those usually reported in the literature. The obtained results are reported in **Fig. 8** and in **Fig. 9**. It can be noticed that for the large load values the convergence of results deteriorates and sufficiently dense meshes are required to obtain a satisfactory convergence. In passing, we would like to point out that we have not been able to finish (in a reasonable time span) the missing parts of load-deformation paths for meshes 20×20 and 30×30 in **Fig. 9**. The respective curves are very difficult to follow since they contain large number of loops.

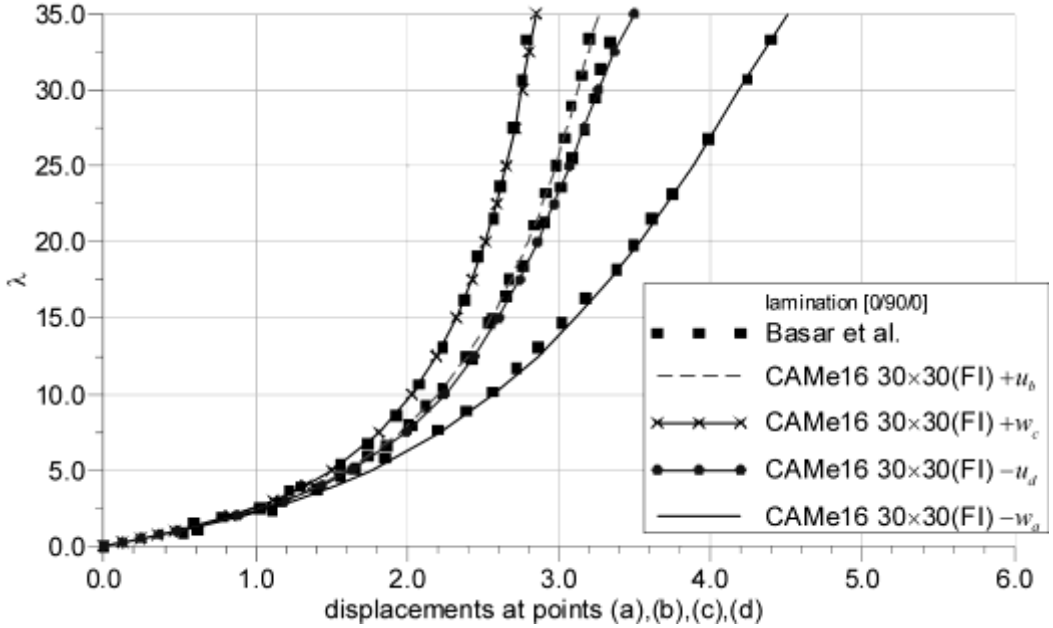

Fig. 6. Hyperboloid shell, results for lamination [0/90/0]

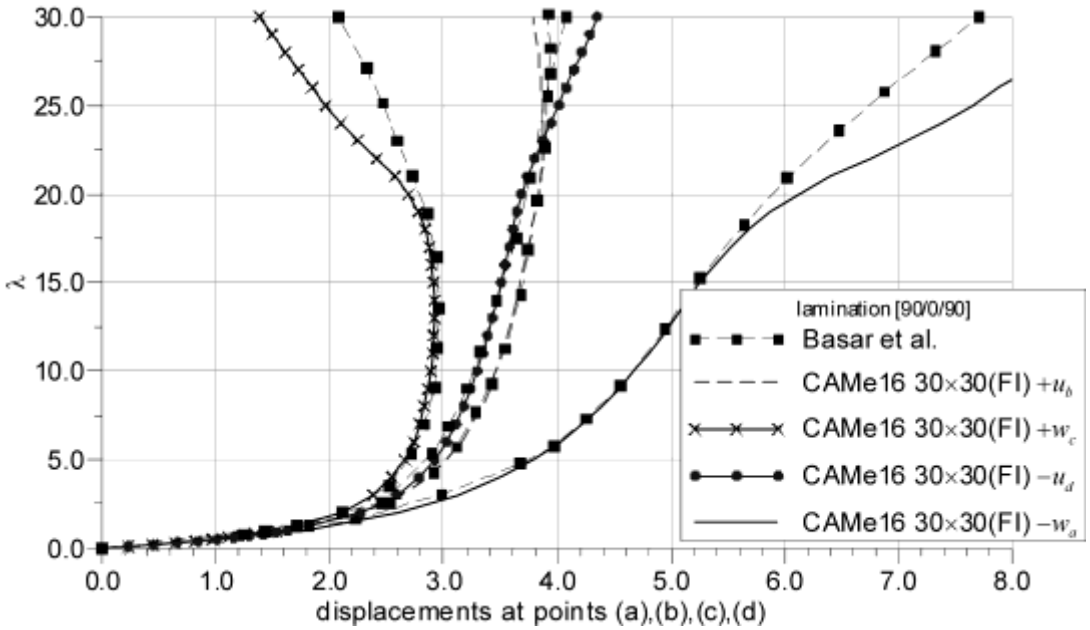

Fig. 7. Hyperboloid shell, results for lamination [90/0/90]

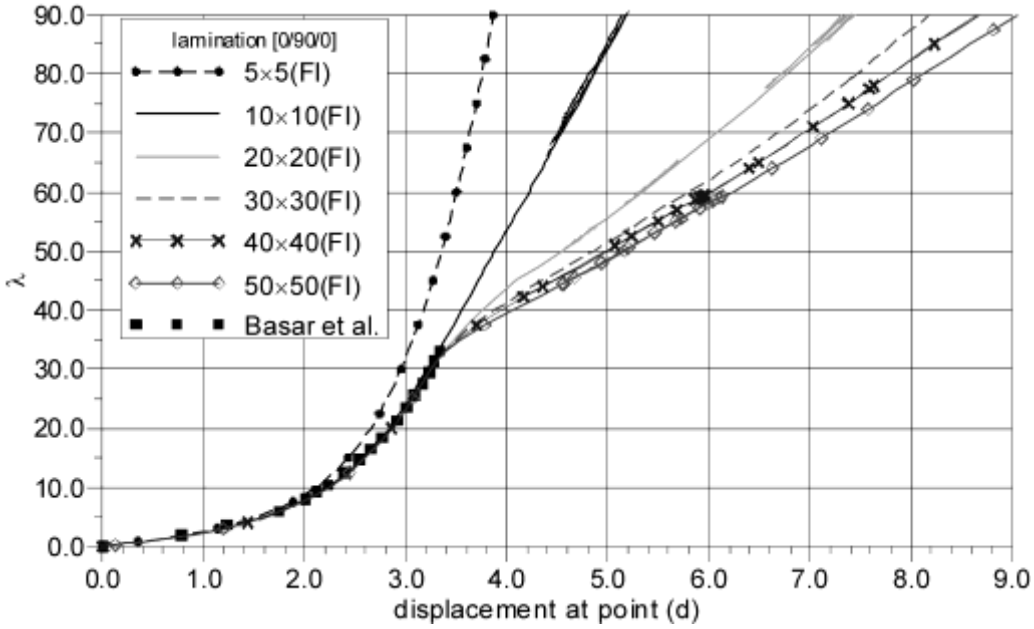

Fig. 8. Hyperboloid shell, nonlinear convergence analysis, results for lamination [0/90/0]

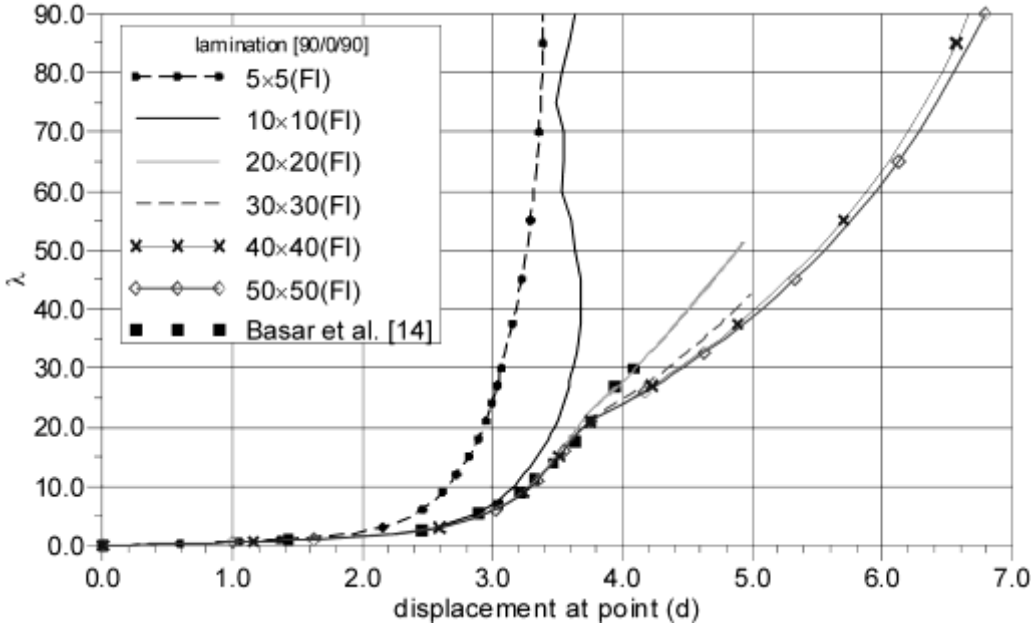

Fig. 9. Hyperboloid shell, nonlinear convergence analysis, results for lamination [90/0/90]

The above results indicate the correctness of the proposed formulation, at least in the range of examples and deformations usually found in the literature. The next examples deal with shell structures that are seldom analyzed. In particular, we concentrate on shells with orthogonal intersections.

4.4. Three layer hyperbolic paraboloid shell

Originally this problem was formulated in [59] as the homogenous isotropic example for testing the large rotation shell theory and the assessment of the element in bending of warped meshes. In addition, this is a demanding test for checking the ability of an element to handle rigid-body modes since, under given loads, substantial portions of the structure undergo (almost) rigid-body motions. In a homogenous isotropic setup this example was studied in [3], [48], [60]. Another version of a hyperbolic paraboloid shell was studied in works by Bathe and his co-workers as the homogenous isotropic structure, see e.g. [7], [58], or [61]. The authors of [61] recommended this example as a good benchmark problem to test shell elements in the context of bending dominated problems. The geometry of the present example is given in Fig. 10, where $a=10$, $c=5$, $\sqrt{2}d=1.25$. The midsurface of the shell is described by the following equation: $z=\frac{c}{2a^2}(y^2-x^2)$, $x\in[-(\sqrt{2}a-d/2),(\sqrt{2}a-d/2)]$, $y\in[-\sqrt{2}a,\sqrt{2}a]$. The orthotropy is specified with respect to the directors defined as

$$\boldsymbol{t}_1^0=\frac{(1+\alpha^2y^2)\boldsymbol{e}_1+\alpha^2xy\,\boldsymbol{e}_2-\alpha x\,\boldsymbol{e}_3}{\sqrt{\left(1+\alpha^2y^2\right)\left(1+\alpha^2(x^2+y^2)\right)}},\qquad \boldsymbol{t}_2^0=\frac{\boldsymbol{e}_2+\alpha y\,\boldsymbol{e}_3}{\sqrt{1+\alpha^2y^2}},\qquad \alpha=\frac{c}{a^2} \tag{32}$$

Note that the director $\boldsymbol{t}_2^0$ Eq. $(32)_2$ always belongs to the $y-z$ plane. This is very important from the engineering viewpoint since it allows one to reinforce the shell with the lines of reinforcement which do not converge, contrary to the finite element mesh used in the example. The load is assumed as the self-equilibrated and proportional $\mathbf{M}_y(\lambda)=\lambda\boldsymbol{M}_{ref}$ with respect to the reference load taken as the moment distributed along the

cut edge $\boldsymbol{M}_{ref} = m_0 \int_0^d ds_0(y)\boldsymbol{e}_2$, $m_0 = 5$. In the composite setup we use the following material data: $E_1 = 10^5$ kN/m^2, $E_2 = \frac{1}{2}E_1 = 0.5\times10^5$ kN/m^2, $G_{12} = G_{13} = G_{23} = 4\times10^4$ kN/m^2, $\nu_{12} = 0.25$. We assume two different cross-ply lamination schemes [90/0/90] and [0/90/0]. The total thickness of the shell is $h = 0.18$ m divided into three layers of the same thickness. For the homogenous isotropic case we take $h = 0.18$ m with two values of Young's modulus $E = 10^5$ kN/m^2 or $E = 0.5\times10^5$ kN/m^2 and $\nu = 0.25$. The latter values are different than in the original formulation. Of course, the linear elastic homogenous isotropic solutions for different values of Young's modulus must be identical, after appropriate scaling proportional to these values. We assume that the shell is free, supported only at the point (c) in the vertical direction z. Due to symmetries only a quarter of the shell is analyzed with appropriate boundary conditions using 8×24 CAMe16 elements, where 24 elements are taken along the x axis.

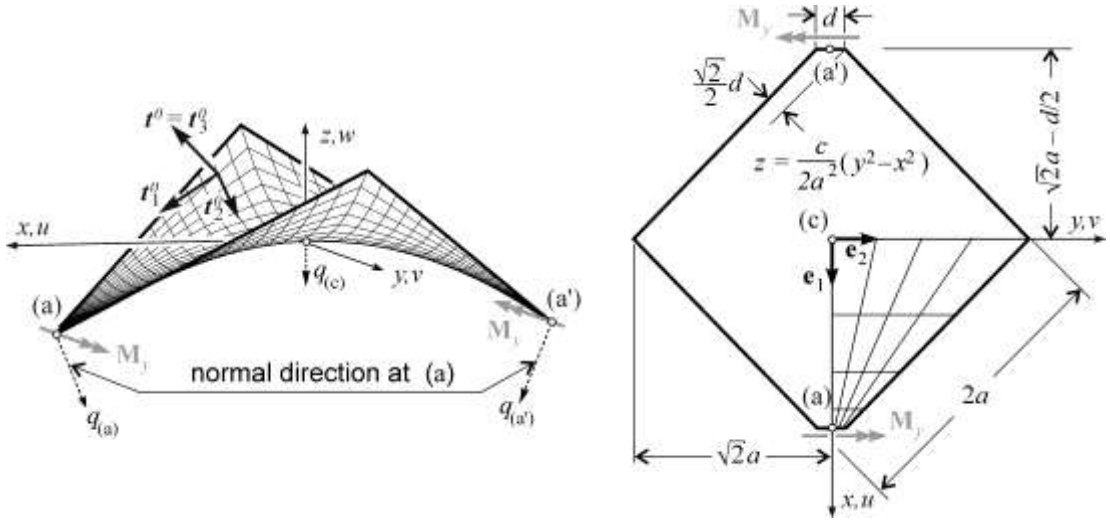

Fig. 10. Hyperbolic paraboloid shell, geometry

The representative results are presented in Fig. 11. Fig. 12 illustrates the deformed meshes of the laminated structure for $\lambda = 16$. The change of lamination scheme, under the considered load, shows that the structure behaves like a homogenous isotropic shell with one of the considered modulus of elasticity. This indicates that in the considered case the influence of the structural rigidity generated by the curvature is relatively small.

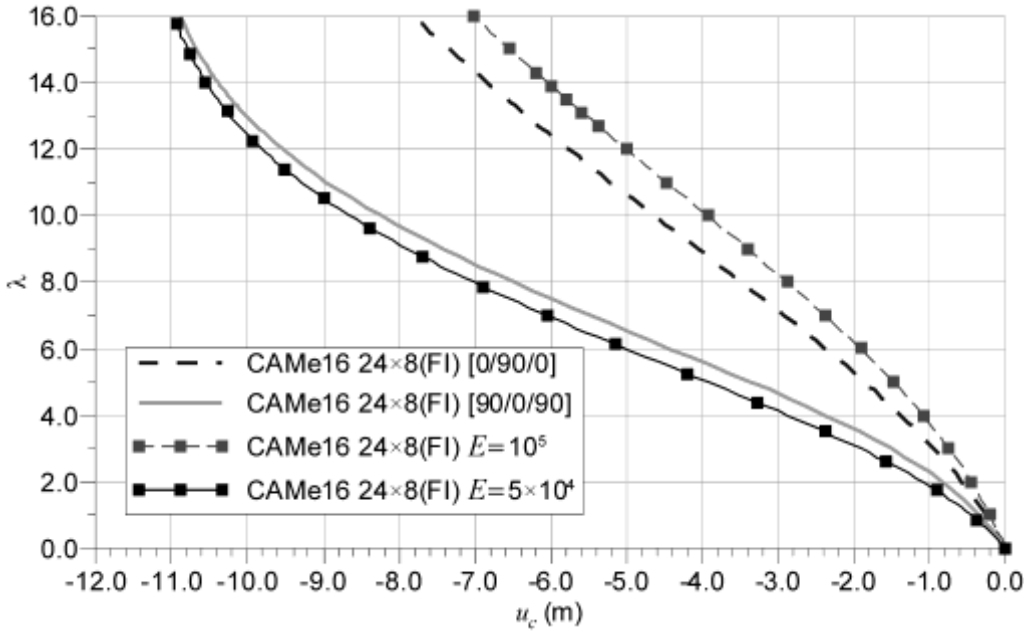

Fig. 11. Hyperbolic paraboloid shell, nonlinear deformation paths

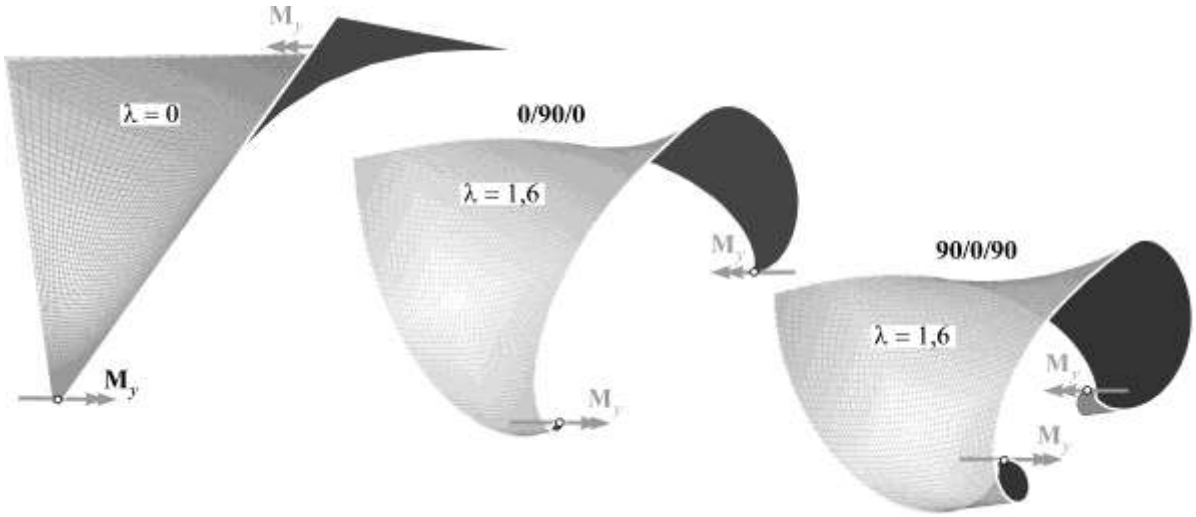

Fig. 12. Hyperbolic paraboloid shell, deformed meshes of laminated structures, λ = 16

4.5. Three layer channel section cantilever

The problem analyzed in this section was originally formulated in [62] as a simply supported beam with uniformly distributed (along the web) load. In [2] it has been reformulated to the cantilever under action of the point load. In such setup it has become a popular benchmark problem for various shell and element formulations in elastic and elasto-plastic analysis, see e.g. [4], **Błąd! Nie można odnaleźć źródła odwołania.**[12], [63], [64], [65], [66]. The solid-shell elements from [65] provide an alternative for modeling the shell junctions. Note that there exists another homogenous isotropic variant of this example, see for instance [4], [8]. The structure analyzed here is depicted in **Fig. 13**. The geometry is described by $L=36$ in, $a=2$ in, $b=6$ in, while the load is assumed as proportional $P(\lambda)=\lambda P_{ref}$ lb with $P_{ref}=100$ lb. We have modified the original thickness from $h=0.05$ in to $h=0.06$ in so that the layers are of the equal thickness 0.02 in. We assume two cross-ply lamination schemes [90/0/90] and [0/90/0] and the material described by $E_1=10^7$ lb/in^2,

$E_2 = 4\times10^5$ lb/in^2, $G_{12} = G_{13} = 2\times10^5$ lb/in^2, $G_{23} = 8\times10^4$ lb/in^2, $\nu_{12} = 0.333$. In the homogenous isotropic case we use $h_0 = 0.06$ in, $E = 0.25\times10^7$ lb/in^2 and $\nu = 0.333$. The value of Young's modulus in this case has been chosen purposely to enable a better comparison of a qualitative behavior of the structure. The mesh of CAMe16 elements used for the computations consists of 4 elements for the upper and the lower flange, 6 elements for the web and 72 elements along the cantilever length.

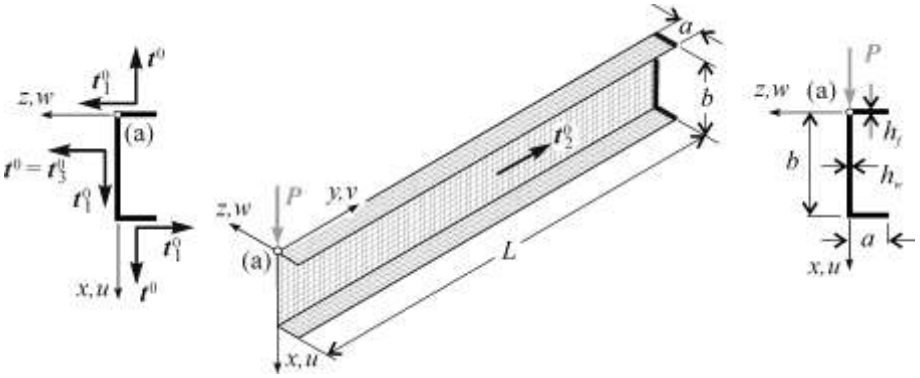

Fig. 13. Channel section cantilever, geometry and load

The nonlinear deformation paths of the translation $u_{(a)}$ are shown in **Fig. 14** and in **Fig. 15** to enlighten the qualitative differences between solutions obtained with different lamination schemes. The presented graphs show the significant influence of the internal structure of the shell material on the overall response of the channel section. In the solution of the homogenous isotropic variant and the composite [0/90/0] variant the limit point is clearly visible, while for the lamination [90/0/90] the limit point almost disappears. However, the latter solution is characterized by the complicated equilibrium path with sudden turns. This indicates that there must appear deformation waves that must be properly reproduced by the sufficiently dense FEM mesh. This issue has been discussed extensively in [4]. **Fig. 16** depicts the deformed configurations of the structure obtained in a well-advanced phase of deformations for the same value of the control translation $u(a) = 5.4$ in. The homogenous isotropic variant and the [0/90/0] laminated variant preserve the shape of the cross-section, yet there appear the deformation waves in the neighborhood of the clamped edge. In the [90/0/90] laminated structure the web collapses.

For comparison purposes, due to a lack of a known reference solution, this example has been also analyzed with the commercial FEA system NX-Nastran [67]. It is worth to point out that while using the *Standard Nonlinear Analysis* option ("solution 106") based on the original Nastran with the QUAD4 elements, we have encountered some convergence problems. Therefore, the NX-Nastran results presented in **Fig. 14** and in **Fig. 15** have been obtained with the *Advanced Nonlinear Analysis* option ("solution 601") utilizing the ADINA solver. The computational model contained 12 CQUAD8 elements for each flange, 27 elements for the web and 216 along the length.

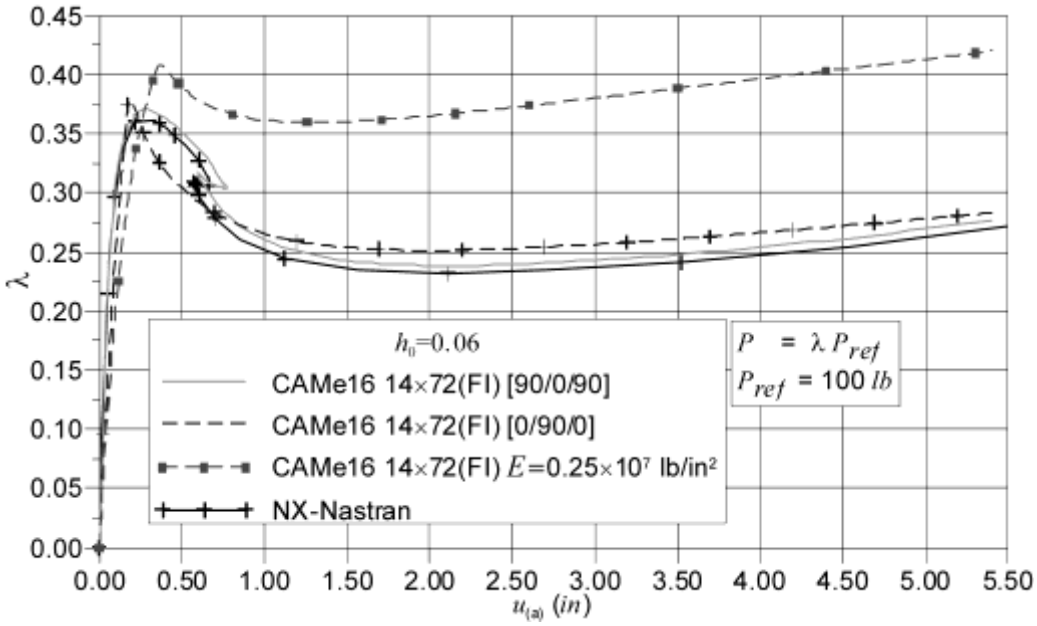

Fig. 14. Channel section cantilever, nonlinear deformation paths

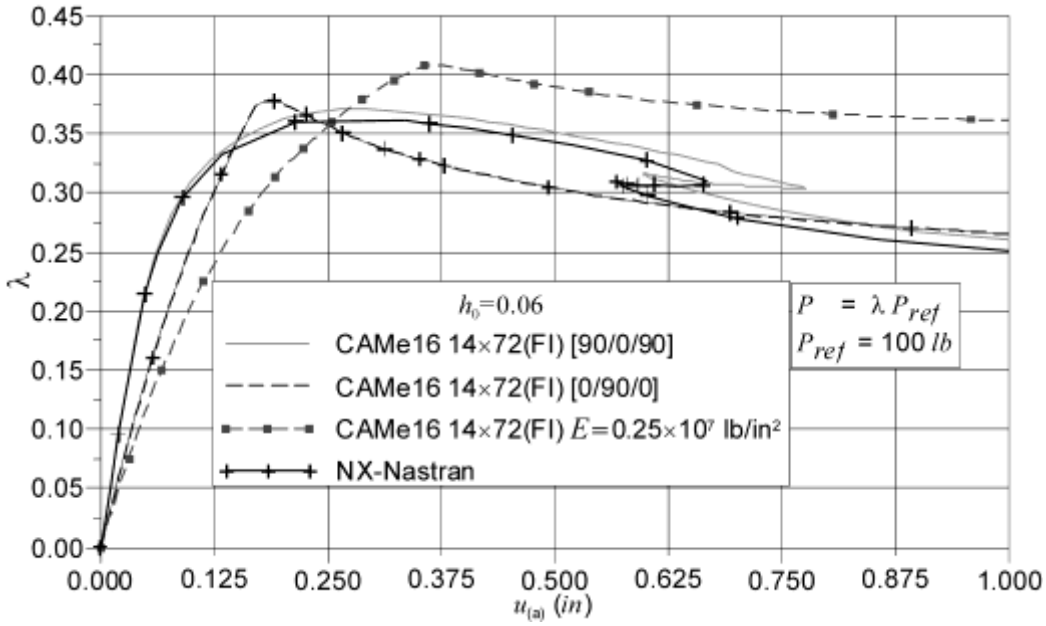

Fig. 15. Channel section cantilever, comparison of nonlinear deformation paths in the vicinity of the limit point

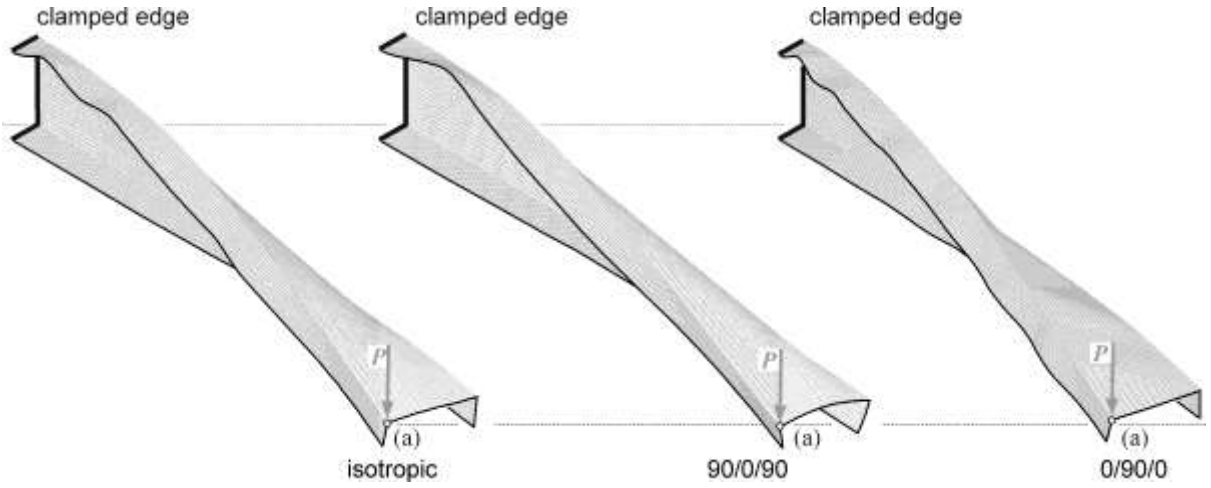

Fig. 16. Channel section cantilever, deformed meshes, u(a) = 5.4 in

4.6. Stiffened doubly curved cylindrical panel

In [3] a structural shell as shown in **Fig. 17** was proposed. The orthogonal intersection together with the change of the curvature make this problem a challenging testing example for any shell element with drilling dof as well as for solution procedures used to trace the equilibrium paths. Dimensions are: $L = 2\,\text{m}$, $\alpha = 45°$, $R = 1$ m, $H = 0.4$ m, $h_0 = 0.01$ m, $P_{ref} = 1\,\text{MN}$, $P(\lambda) = \lambda P_{ref}$. We analyze two lamination schemes [90/0/0/90] and [0/90/90/0] with $E_1 = 10^5$ MPa, $E_2 = 7\times10^3$ MPa, $G_{12} = G_{13} = 4\times10^3$ MPa, $G_{23} = 3.2\times10^3$ MPa, $\nu_{12} = 0.25$.
The mesh of CAMe16 elements used in the analysis consists of 10 elements per each flange, 4 elements for the web and 12 along the length of the structure. The results are depicted in **Fig. 18**. The graphs, obtained using arc-length procedure, show significant difference between the responses of the structure for different laminations. Only for small values of load the graphs coincide. Some representative deformed configurations for λ = 0.0804374 in case of lamination [0/90/90/0] and λ = 0.113801 for [90/0/0/90] are marked by dots in **Fig. 18** and are depicted in **Fig. 19**.

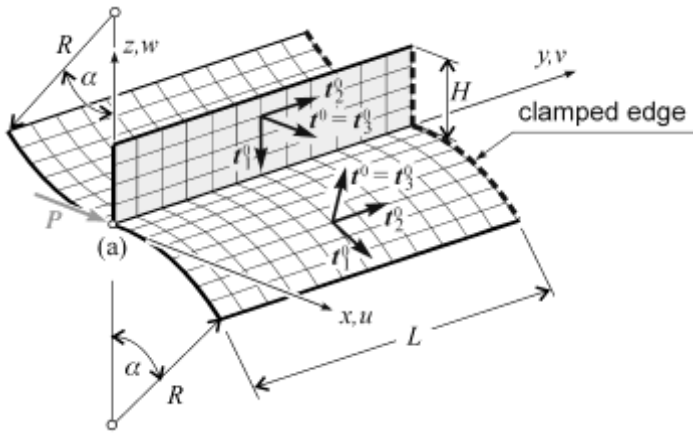

Fig. 17. Stiffened doubly curved cylindrical panel, geometry

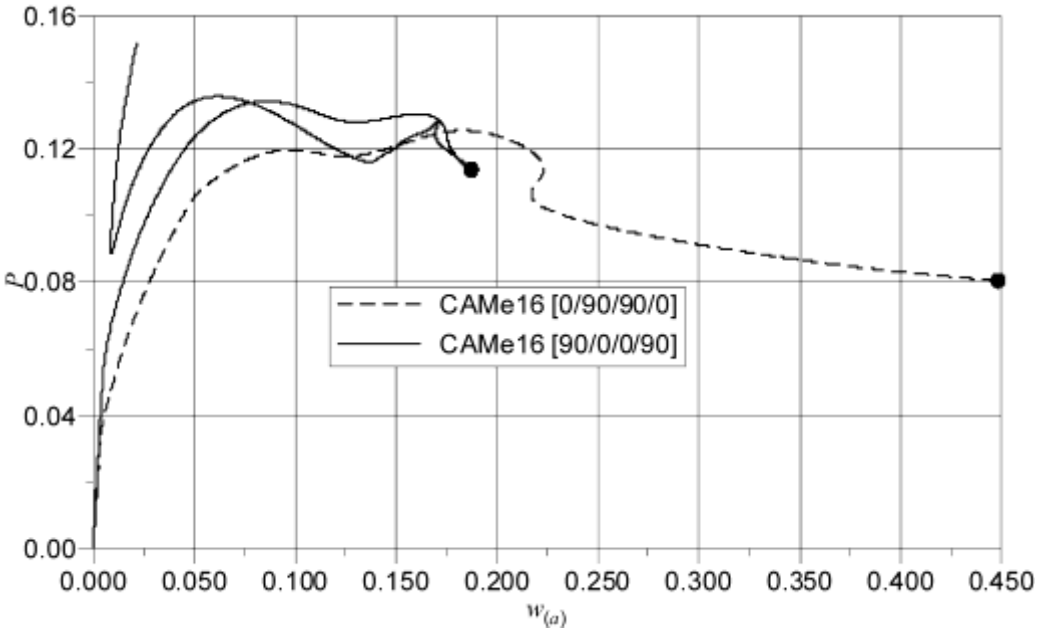

Fig. 18. Stiffened doubly curved cylindrical panel, load-displacement curves

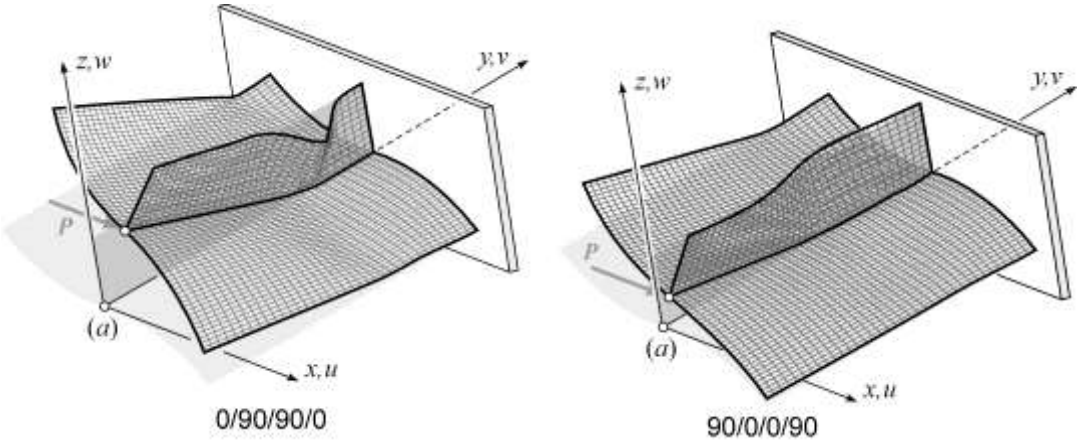

Fig. 19. Stiffened doubly curved cylindrical panel, deformed configurations

5. CONCLUSIONS

In this paper, the composite shell formulation within the framework of the 6-parameter nonlinear general shell theory with drilling degrees of freedom has been presented. Assuming the ESL model, a material law has been derived as the straightforward extension of constitutive equations known for classical 5-parameter shell models. The proposed methodology enables a direct use of engineering constants for classical orthotropic continuum.

The proposed material law has been implemented in the displacement (translation-rotation) based elements that stem from the underlying governing principle of virtual work of the discussed shell theory. Therefore, additional variables, such as those emanating from multi-field variational principles, do not appear. In order to minimize the locking effect always present in pure translation-rotation based elements and to omit discussion about elimination of locking, we have used 16-node elements with relatively dense meshes.

The presented results allow us to formulate the following conclusions:

- it is possible to extend the material equations known for 5-parameter laminated shell theory to accommodate asymmetric membrane and bending strain measures,
- the proposed methodology of computing material coefficients has been proven satisfactory, since in the comparison with the examples that can be solved using 5-parameter shell theory, the results obtained on the grounds of the present shell formulation are in a very good agreement,
- the presented formulation is also capable of including a composite structure of the shell material in the irregular structures possessing folds, branches and intersections.

ACKNOWLEDGEMENTS

The financial support from the Polish Ministry of Science and Higher Education is acknowledged (grant no. N N506 254237)

APPENDIX 1 INTERPOLATION ON SO(3) GROUP

The interpolation scheme, as described by Eq.(12), is not available (with all the necessary mathematical formalism) for $SO(3)$-valued functions $\boldsymbol{Q}(\xi)$, $\boldsymbol{T}_0(\xi) \Rightarrow \{\boldsymbol{t}_i^0(\xi)\}$ and $\boldsymbol{T}(\xi) = \boldsymbol{Q}(\xi)\boldsymbol{T}_0(\xi) \Rightarrow \{\boldsymbol{t}_i(\xi)\}$. In the present formulation, we employ the indirect C^0 interpolation that is based on a transport of the approximation domain into the neighborhood of the neutral element $\mathbf{1} \in SO(3)$, where interpolation error grows at the slowest rate. The procedure on $SO(3)$ consists of the following steps:

1. Establishing for the set $\boldsymbol{Q}_a \in U \subset SO(3)$ a constant, average representative tensor $\bar{\boldsymbol{Q}} \in SO(3)$.
2. Transporting the set $\boldsymbol{Q}_a$ into the neighborhood of $\mathbf{1} \in W \subset SO(3)$ by the kind of pull back with $\bar{\boldsymbol{Q}}$, that is creating a set of nodal tensors $\boldsymbol{R}_a = \bar{\boldsymbol{Q}}^{\mathrm{T}}\boldsymbol{Q}_a$.
3. Introducing three chosen (say Cayley, canonical, Euler) local parameters $\boldsymbol{R}_a \xrightarrow{\mathrm{R}} (\varpi_p)_a$, $(\varpi_p)_a = \mathrm{R}(\boldsymbol{R}_a)$ in the map (W, R). Note that the parametrization considered here does not have to be the same as the parametrization used in this paper, i.e. canonical.
4. Interpolating three scalar functions $\varpi_p(\xi) \in R^3$ through the nodal values $(\varpi_p)_a$ according to Eq. (12).
5. Calculating the interpolating tensor function $\tilde{\boldsymbol{R}}(\xi) = \mathrm{R}^{-1}\left(\varpi_p(\xi)\right) \in W \subset SO(3)$.
6. Transporting back the tensor function $\tilde{\boldsymbol{R}}(\xi)$ into the initial position in $U \subset SO(3)$ by the kind of push-forward operation with $\bar{\boldsymbol{Q}}$: $W \to U \subset SO(3)$, $\tilde{\boldsymbol{Q}}(\xi) = \bar{\boldsymbol{Q}}\tilde{\boldsymbol{R}}(\xi)$

The concept of the procedure is portrayed in Fig. 20. Consequently, $\tilde{\boldsymbol{Q}}(\xi)$ interpolates the given function $\boldsymbol{Q}(\xi) \in C(\pi_{(e)}, SO(3))$ at the set of nodes $\xi_a \in \pi_{(e)}$. From $\tilde{\boldsymbol{Q}}(\xi) = \bar{\boldsymbol{Q}}\tilde{\boldsymbol{R}}(\xi)$ it also follows that the interpolating function $\tilde{\boldsymbol{Q}}(\xi)$ always takes on the values in the rotation group $SO(3)$. Within finite elements, the proposed interpolation procedure practically removes any singularity which may follow from a local parameterization. The above scheme is used here for all $SO(3)$-valued functions, such as $\boldsymbol{Q}(\xi)$, $\boldsymbol{T}_0(\xi)$ and $\boldsymbol{T}(\xi)$.

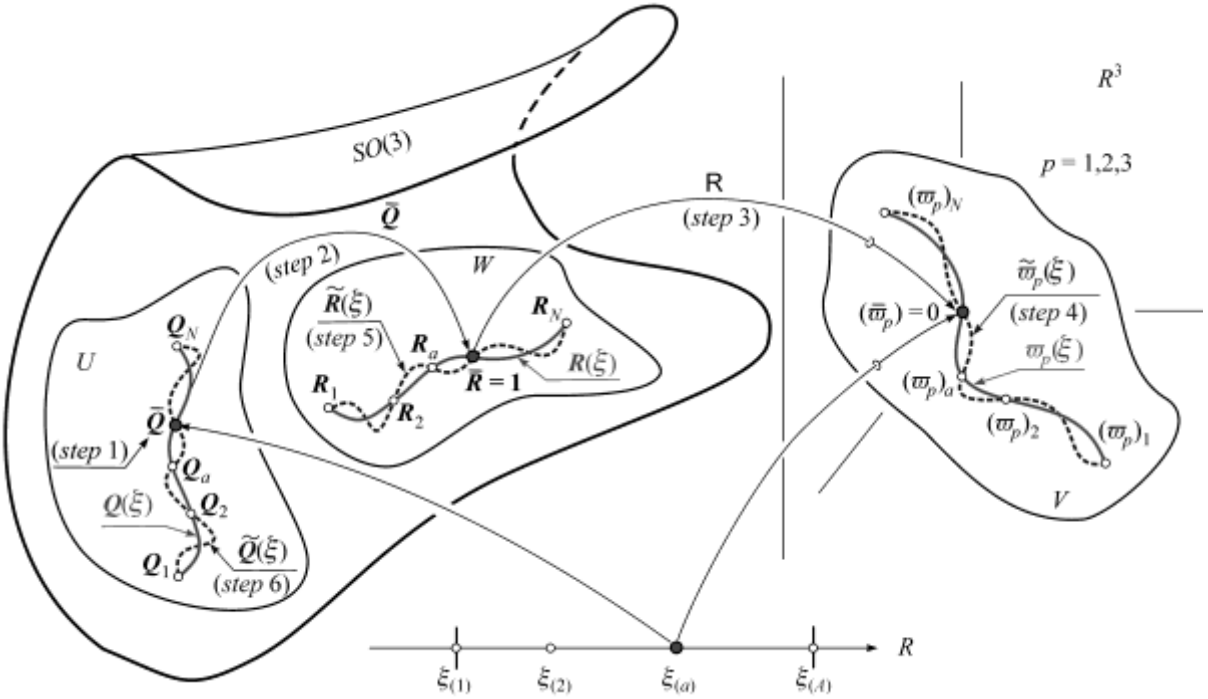

Fig. 20. Concept of interpolation on *SO*(3)

REFERENCES

[1] J. Chróścielewski, J. Makowski, W. Pietraszkiewicz, Statics and Dynamics of Multifold Shells: Nonlinear Theory and Finite Element Method, (in Polish), Institute of Fundamental Technological Research Press, Warsaw, 2004.

[2] J. Chróścielewski, J. Makowski, H. Stumpf, Genuinely resultant shell finite elements accounting for geometric and material non-linearity, International Journal for Numerical Methods in Engineering, vol. 35, pp. 63–94, 1992.

[3] J. Chróścielewski, J. Makowski, H. Stumpf, Finite element analysis of smooth, folded and multi-shell structures, Comp. Meth. Appl. Mech. Engng., vol. 141, pp. 1-46, 1997.

[4] J. Chróścielewski, W. Witkowski, 4-node semi-EAS element in 6–field nonlinear theory of shells, International Journal for Numerical Methods in Engineering, vol. 68, pp. 1137–1179, 2006. DOI: 10.1002/nme.1740.

[5] E. Reissner, Linear and nonlinear theory of shells, in Y.C. Fung, and E.E. Sechler (eds.), Thin Shell Structures, 29-44, Prentice-Hall, Englewood Cliffs, 1974.

[6] A. Libai, J. G. Simmonds, The Nonlinear Theory of Elastic Shells, Cambridge University Press, 1998.

[7] K.J. Bathe, A. Iosilevich, D. Chapelle, An evaluation of the MITC shell elements, Computers and Structures, vol. 75, pp. 1-30, 2000.

[8] W. Wagner, F. Gruttmann, A robust non-linear mixed hybrid quadrilateral shell element, International Journal for Numerical Methods in Engineering, vol. 64, pp. 635-666, 2005. DOI: 10.1002/nme.1387.

[9] G.M. Kulikov, S.V. Plotnikova, Equivalent single-layer and layer-wise shell theories and rigid-body motions - Part I: Foundations, Mech. Advanced Mater. Struct., vol. 12, pp. 275- 283, 2005.

[10] M. Bischoff, W.A. Wall, K.W. Bletzinger, E. Ramm, Models and finite elements for thin-walled structures, in E. Stein, R. de Borst, T.J.R. Hughes (eds.), Encyclopedia of Computational Mechanics. Vol. 2: Solids and Structures, pp. 59-137, Willey, 2004.

[11] A. Ibrahimbegović, F. Frey, Stress Resultant Geometrically Nonlinear Shell Theory With Drilling Rotations. Part I: Theoretical Formulation, Computer Methods in Applied Mechanics and Engineering, vol. 118, pp. 265-284, 1994.

[12] A. Ibrahimbegović, F. Frey, Stress resultant geometrically nonlinear shell theory with drilling rotations - Part II: Computational aspects, Comp. Meth. Appl. Mech. Engng, vol. 118, pp. 285-308, 1994.

[13] A. Ibrahimbegović, F. Frey, Stress Resultant Geometrically Nonlinear Shell Theory With Drilling Rotations. Part III: Linearized Kinematics, Journal for Numerical Methods in Engineering, vol. 37, pp. 3659-3683, 1994.

[14] A. Ibrahimbegović, Stress Resultant Geometrically Exact Shell Theory for Finite Rotations and Its Finite Element Implementation, ASME Applied Mechanics Reviews, vol. 50, pp. 199-226, 1997.

[15] C. Sansour and H. Bednarczyk: The Cosserat surface as a shell model, theory and finite-element formulation, Computer Methods in Applied Mechanics & Engineering, vol. 120, pp. 1-32, 1995.

[16] C. Sansour and J. Boćko: On hybrid stress, hybrid strain and enhanced strain finite element formulations for a geometrically exact shell theory with drilling degrees of freedom, Int. Journal for Numerical Methods in Engineering vol. 43, 175-192, 1998.

[17] A. Ibrahimbegovic, B. Brank, P. Courtois, Vector-like Parameterization on Constrained Finite Rotations for Smooth Shells, International Journal for Numerical Methods in Engineering, vol. 52, pp. 1235-1252, 2001.

[18] C. Sansour and W. Wagner: Multiplicative updating of the rotation tensor in the finite element analysis of rods and shells – a path independent approach, Computational Mechanics 31, 153-162, 2003.

[19] A. Ibrahimbegović, Nonlinear shell theory with finite rotations and finite strains: recent achievements, in W. Pietraszkiewicz, and C. Szymczak (eds.), Shell Structures: Theory and Applications, pp. 19-33, Taylor & Francis/Balkema, London, 2005.

[20] A. Ibrahimbegović, J.B. Colliat, L. Davenne, Thermomechanical coupling in folded plates and non-smooth shells, Computer Methods in Applied Mechanics and Engineering, vol. 194, pp. 2686-2707, 2005.

[21] P.Panasz, K. Wiśniewski, Nine-node shell elements with 6 dofs/node based on two-level approximations. Part I Theory and linear tests, Finite Elements in Analysis and Design, vol. 44, pp. 784–796, 2008.

[22] I. Kreja, R. Schmidt, J. N. Reddy, Finite elements based on a first-order shear deformation moderate rotation shell theory with applications to the analysis of composite structures, International Journal of Non-Linear Mechanics, vol. 32, pp. 1123–1142, 1997.

[23] I. Kreja and R. Schmidt: Large rotations in First Order Shear Deformation FE analysis of laminated shells, Int. Journal Non-Linear Mechanics 41, 101-123, 2006.

[24] E. Carrera, Developments, ideas, and evaluations based upon Reissner's Mixed Variational Theorem in the modeling of multilayered plates and shells, Appl Mech Rev, vol 54(4), pp. 301-329, 2001.

[25] J. N. Reddy and R. A. Arciniega: Shear deformation plate and shell theories: From Stavsky to Present, Mechanics of Advanced Materials and Structures 11, 535-582, 2004.

[26] I. Kreja, Geometrically non-linear analysis of layered composite plates and shells, vol. 83, pp. 1-176, Monographs of Gdansk University of Technology, Gdańsk, 2007.

[27] V. V. Vasiliev, E. V. Morozov, Mechanics and Analysis of Composite Materials, pp. 225-269, Elsevier Science Ltd, Oxford, 2001.

[28] Y. Başar, Y. Ding, R. Schultz, Refined shear deformation models for composite laminates with finite rotations, International Journal of Solids and Structures, vol. 30(19), pp. 2611-38, 1993.

[29] H. Altenbach, On the determination of transverse shear stiffnesses of orthotropic plates, Z. angew. Math. Phys., vol. 51, pp. 629-649, 2000.

[30] V. Konopińska, W. Pietraszkiewicz, Exact resultant equilibrium conditions in the non-linear theory of branching and self-intersecting shells, International Journal of Solids and Structures, vol. 44, pp. 352–369, 2007.

[31] R. D. Mindlin, Stress functions for a Cosserat continuum, International Journal of Solids and Structures, vol. 1, pp. 265-271, 1965.

[32] W. Nowacki, Theory of asymmetric elasticity, Pergamon Press, Oxford, 1986.

[33] A. C. Eringen, Theory of micropolar elasticity, in Liebowitz (eds.), Fracture, pp 621-729, Academic Press, 1968.

[34] J. Chróścielewski, Family of C^0 finite elements in six parameter nonlinear theory of shells (in Polish), Proceeding of Gdansk Technical University, Civil Eng. Series, vol. **540**(LIII), pp. 1–291, 1996.

[35] J. Chróścielewski, J. Makowski, W. Pietraszkiewicz, Non-linear dynamics of flexible shell structures, Computer Assisted Mechanics and Engineering Science, vol. 9, pp. 341-357, 2002.

[36] S. C. Cowin, An incorrect inequality in micropolar elasticity theory, J. Appl. Mech. Phys., vol. 21, pp. 494–497, 1970.

[37] S. Nakamura, R. S. Lakes, Finite element analysis of Saint-Venant end effects in micropolar elastic solids, Engineering Computations, vol. 12, pp. 571–587, 1995.

[38] E. Providas, M. A. Kattis, Finite element method in plane Cosserat elasticity, Computers and Structures, vol. 80, pp. 2059–2069, 2002.

[39] V.A. Eremeyev, W. Pietraszkiewicz, Local symmetry group in the general theory of elastic shells, Journal of Elasticity, vol. 85, pp. 125-152, 2006.

[40] R. D. Gauthier, W. E. Jahsman, A quest for micropolar elastic constants, J. Applied Mechanics, vol. 42, pp. 369–374, 1975.

[41] R. D. Gauthier, W. E. Jahsman, A quest for micropolar elastic constants, part II, Arch. Mech., vol. 33, pp. 717–737, 1981.

[42] A.E. Green, P.M. Naghdi, A theory of laminated composite plates, IMA J. Appl. Math., vol. 29, pp. 1-23, 1982.

[43] S. Nakamura, R. Benedict, R. Lakes, Finite element method for orthotropic micropolar elasticity, International Journal of Engineering Science, vol. 22 (3), pp. 319–330, 1984.

[44] S. Casolo, Macroscopic modelling of structured materials. Relationship between orthotropic Cosserat continuum and rigid elements, International Journal of Solids and Structures, vol. 43, pp. 475–496, 2006.

[45] M. Bîrsan, On Saint–Venant's problem for anisotropic, inhomogeneous, cylindrical Cosserat elastic shells, International Journal of Engineering Science, vol. 47, pp. 21–38, 2009.

[46] E. Ramm, From Reissner plate theory to three dimensions in large deformations shell analysis, ZAMM, vol. 80, pp. 61-68, 2000.

[47] L. Vu-Quoc, X. G. Tan, Optimal solid shells for non-linear analyses of multilayer composites. I. Statics, Comp. Meth. Appl. Mech. Engng., vol. 192, pp. 975–1016, 2003.

[48] N. Stander, A. Matzenmiller, E. Ramm, An assessment of assumed strain methods in finite rotation shell analysis, Engineering Computations, vol. 6, pp. 58–66, 1989.

[49] S. Klinkel, F. Gruttmann, W. Wagner, A continuum based three-dimensional shell element for laminated structures, Computers and Structures, vol. 71, pp. 43–62, 1999.

[50] K. Y. Sze, X. H. Liu, S. H. Lo, Popular benchmark problems for geometric nonlinear analysis of shells, Fin. Elem. Anal. Des., vol. 40, pp. 1151–1569, 2004.

[51] R. A. Arciniega, J. N. Reddy, Tensor-based finite element formulation for geometrically nonlinear analysis of shell structures, Comput. Methods Appl. Mech. Engrg., vol. 196, pp. 1048–1073, 2007.

[52] A. K. Noor, S. J. Hartley, Nonlinear shell analysis via mixed isoparametric elements, Computers and Structures, vol. 7, pp. 615–626, 1977.

[53] A. F. Palmerio, J. N. Reddy, R. Schmidt, On moderate rotation theory of laminated anisotropic shells – part 2. Finite element analysis, International Journal of Non-Linear Mechanics, vol. 25, pp. 701-714, 1990.

[54] C. L. Liao, and J. N. Reddy, An incremental total Lagrangian formulation for general anisotropic structures, Report No. CCMS-87-16, Virginia Polytechnic Institute and State University, Blacksburg, VA, 1987.

[55] W. Wagner, F. Gruttmann, A simple finite rotation formulation for composite shell elements, Engineering Computations, vol. 11, pp. 145-76, 1994.

[56] M. Balach, H. N. Al-Ghamedy, Finite element formulation of a third order laminated finite rotation shell element, Computers and Structures, vol. 80, pp. 1975–1990, 2002.

[57] D. Chapelle, K. J. Bathe, The finite element analysis of shells–Fundamentals, Springer-Verlag, Berlin, 2003.

[58] P. S. Lee, K. J. Bathe, Insight into finite element shell discretizations by use of the ‘‘basic shell mathematical model’’, Computers and Structures, vol. 83, pp. 69–90, 2005.

[59] Y. Başar, Y. Ding, Finite rotation elements for the non-linear analysis of thin shell structures, International Journal of Solids and Structures, vol. 26, pp. 83-97, 1990.

[60] P. Wriggers, F. Gruttmann, Thin shells with finite rotations formulated in Biot stresses: Theory and finite element formulation, International Journal for Numerical Methods in Engineering, vol. 36, pp. 2049-2071, 1993.

[61] P. S. Lee, K. J. Bathe, On the asymptotic behavior of shell structures and the evaluation in finite element solutions, Computers and Structures, vol. 80, pp. 235-255, 2002.

[62] H. P. Lee, P. J. Haris, Post-buckling strength of thin-walled members, Computers and Structures, vol. 10, pp. 689-702, 1979.

[63] P. Betsh, F. Gruttmann, E. Stein, A 4–node shell element for the implementation of general hyperelastic 3D–elasticity at finite strains, Comput. Methods. Appl. Mech. Engrg, vol. 130, pp. 57-79, 1996.

[64] R. Eberlein, P. Wriggers, Finite element concepts for finite elastoplastic strain and isotropic stress response in shells: theoretical and computational analysis, Comp. Meth. Appl. Mech. Engng, vol. 171, pp. 243-279, 1999.

[65] X.G. Tan, L. Vu-Quoc, Efficient and accurate multilayer solid-shell element: Non-linear materials at finite strain, International Journal for Numerical Methods in Engineering, vol. 63, pp. 2124–2170, 2005.

[66] S. Klinkel, F. Gruttmann, W. Wagner, A mixed shell formulation accounting for thickness strains and finite strain 3d material models, International Journal for Numerical Methods in Engineering, vol. 74, pp. 945–970, 2008.

[67] NX-Nastran 6.0